


ORIGINAL ARTICLE

Constraining the process of intracontinental subduction in the Austroalpine Nappes: Implications from petrology and Lu-Hf geochronology of eclogites

Irena Miladinova^{1,2}  | Nikolaus Froitzheim¹ | Thorsten J. Nagel³ | Marian Janák⁴ | Raúl O. C. Fonseca⁵ | Peter Sprung⁶ | Carsten Münker⁷

¹Institute of Geosciences, University of Bonn, Bonn, Germany

²Institute of Earth Sciences, NAWI Graz Geocenter, University of Graz, Graz

³Department of Geoscience, University of Aarhus, Aarhus C, Denmark

⁴Earth Science Institute, Slovak Academy of Sciences, Bratislava, Slovakia

⁵Institute of Mineralogy, Geology and Geophysics, Ruhr-University Bochum, Bochum, Germany

⁶Hot Laboratory (AHL), Paul Scherer Institut (PSI), Villigen, Switzerland

⁷Institut für Geologie und Mineralogie, University of Cologne, Cologne, Germany

Correspondence

Irena Miladinova, Institute of Geosciences, University of Bonn, Meckenheimer Allee 169, Bonn 53115, Germany.
Email: irena.miladinova@uni-graz.at

Funding information

German Science Foundation (DFG), Grant/Award Number: FR700/17-1; Slovak Research and Development Agency, Grant/Award Number: APVV-18-0107

Abstract

High- and ultrahigh-pressure rocks occur in the Austroalpine Nappes in a ~400 km long belt from the Texel Complex in the west to the Siegraben Unit in the east. Garnet growth during pressure increase was dated using Lu-Hf chronometry. The results range between c. 100 and 90 Ma, indicating a short-lived period of subduction. Combined with already published data, our estimates of metamorphic conditions indicate a field gradient with increasing pressure and temperature from the northwest to the southeast, where the rocks experienced ultrahigh-pressure metamorphism. The P-T conditions of the eclogites generally lie on the 'warm' side of the global range of subduction-zone metamorphic conditions. The oldest Cretaceous eclogites (c. 100 Ma) are found in the Saualpe-Koralpe area derived from widespread gabbros formed during Permian to Triassic rifting. In the Texel Complex garnets showing two growth phases yielded a Variscan-Eoalpine mixed age indicating re-subduction of Variscan eclogite-bearing continental crust during the Eoalpine orogeny. Jurassic blueschist-facies metamorphism at Meliata in the Western Carpathians and Cretaceous eclogite-facies metamorphism in the Austroalpine are separated by a time gap of c. 50 Ma and therefore do not represent a transition from oceanic to continental subduction but rather separate events. Thus, we propose that subduction initiation was intracontinental at the site of a Permian rift.

KEYWORDS

Eastern Alps, Eoalpine (Cretaceous) event, high-pressure metamorphism, thermodynamic modelling, Lu-Hf geochronology

1 | INTRODUCTION

Two general scenarios have been proposed for the physical mechanism of nucleation of subduction zones:

spontaneous, that is, caused by gravitational instability of oceanic lithosphere, and induced, that is, resulting from compressive stress acting on a plate (Stern, 2004). According to the prevalent view, subduction begins

This is an open access article under the terms of the Creative Commons Attribution-NonCommercial License, which permits use, distribution and reproduction in any medium, provided the original work is properly cited and is not used for commercial purposes.

© 2021 The Authors. *Journal of Metamorphic Geology* published by John Wiley & Sons Ltd.

within an oceanic plate. However, in the presently active intracontinental belts of Central Asia, i.e., Pamir and Tien Shan mountain ranges, it appears that subduction was initiated within a pre-existing zone of weakness in the Asian continental lithosphere, in response to the compressive stress caused by India-Asia collision to the south (e.g., Burtman & Molnar, 1993; Hamburger et al., 1992; Poupinet et al., 2002; Sobel et al., 2013). According to the same authors evidence of preceding, long-lasting subduction of oceanic lithosphere is lacking.

The Austroalpine (or Eoalpine) high-pressure belt of the Eastern Alps is another candidate for intracontinental subduction initiation (Janák et al., 2004; Stüwe & Schuster, 2010); however, robust data supporting this interpretation is lacking. This zone extends over a distance of ~400 km from the Texel Complex in the west to the Siegraben Unit in the east (Figure 1). It comprises basement rock complexes that were subducted to eclogite-facies and locally ultrahigh-pressure (UHP) conditions in the Late Cretaceous (e.g., Hoinkes et al., 1991;

Janák et al., 2015; Miller, 1990; Miller & Thöni, 1997; Tenczer & Stüwe, 2003; Thöni & Jagoutz, 1992; Thöni & Miller, 1996). Dating of the high-pressure (HP) rocks indicated that the pressure peak was reached at c. 91 Ma, followed by rapid exhumation (Miller, Mundil, et al., 2005; Miller, Thöni, et al., 2005; Thöni et al., 2008; Wiesinger et al., 2006). One hypothesis is that the Austroalpine high-pressure metamorphism is related to the south- or southeast-dipping subduction zone which consumed the Meliata-Hallstatt Ocean. Subduction initiated around 170 Ma and, after collision with the Austroalpine passive continental margin, resulted in stacking of the Austroalpine nappes since 135 Ma (Froitzheim et al., 1996; Neubauer et al., 2000; Neubauer, Dallmeyer, et al., 1999; Thöni & Jagoutz, 1993). A second, younger southeast-directed subduction of the Penninic domain caused the emplacement of the Austroalpine nappe stack on the Penninic rocks.

An alternative hypothesis explaining the geodynamic evolution of the Austroalpine domain in the Eastern Alps

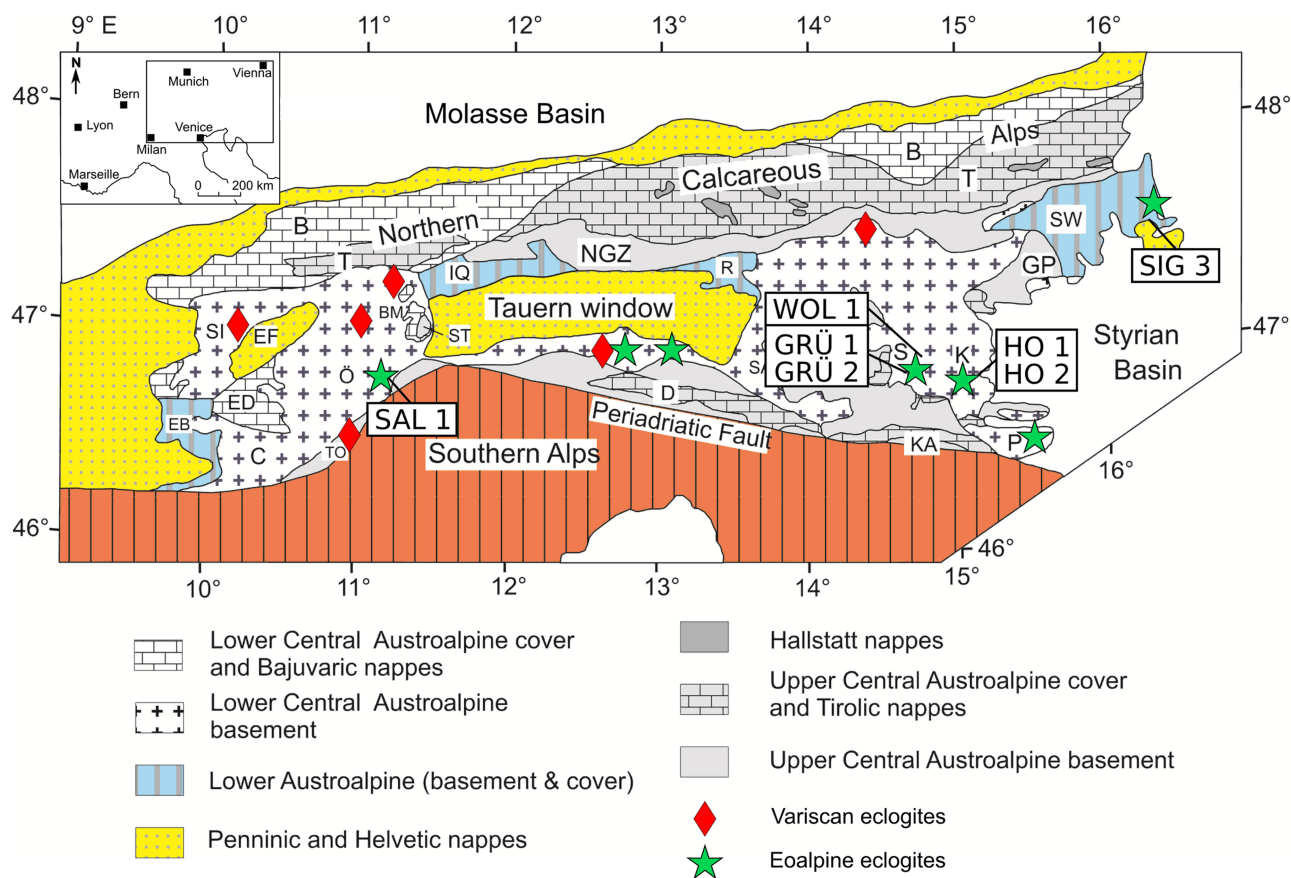


FIGURE 1 Tectonic map of the Eastern Alps modified after Janák et al. (2004), Neubauer and Höck (2000), and Schmid et al. (2004). B, Bajuvaric; BM, Brenner Mesozoic; C, Campo Nappe; D, Drauzug; EB, Err and Bernina Nappes; ED, Engadine Dolomites; EF, Engadine Window; GN, Gurktal Nappe; GP, Graz Paleozoic; IQ, Innsbruck Quartz Phyllite; K, Koralpe; KA, Karawanken; NGZ, Northern Grauwackenzone; Ö, Ötztal Nappe; P, Pohorje Massif; R, Radstadt Nappes; S, Saualpe; SA, Stangalm Mesozoic; SI, Silvretta Nappe; ST, Steinach Nappe; SW, Semmering and Wechsel nappes; T, Tirolic; TO, Tonale Nappe [Color figure can be viewed at wileyonlinelibrary.com]

is the mechanism of ablative subduction, proposed by Polino et al. (1990) and Roda et al. (2012). In this view, the HP/UHP metamorphism occurred by tectonic erosion in the Austroalpine hanging wall of the southeast-dipping subduction zone which consumed the Penninic Ocean. The numerical model of Roda et al. (2012), which assumed a hydrated mantle wedge in an ocean-continent subduction system, was unable to reproduce the high T/P conditions reflected by the natural Austroalpine eclogite sample suite. Roda et al. (2012) suggested modification of several factors to improve the robustness of their numerical models, e.g., variation of the oceanic and/or upper plate thickness, variation of the subduction rate and/or the slab dip, the initial thermal state of the passive margin, the occurrence of continental collision, or an oblique subduction.

Janák et al. (2004) suggested intracontinental subduction as an alternative interpretation of the tectonic and metamorphic evolution of the Austroalpine. According to this model, the north-western parts of the Austroalpine domain (Lower Central Austroalpine) represented the footwall that was subducted under the south-eastern parts (Upper Central Austroalpine), forming the hanging wall. The site of the subduction zone can be traced along the east-west trending zone of Eoalpine high-pressure metamorphic rocks. The subduction was initiated in the NW foreland of the Meliata suture, most probably within a pre-existing Permian-age rift that was reactivated when convergence across the suture continued after the closing of the Meliata Ocean (Janák et al., 2004; Kurz & Fritz, 2003; Stüwe & Schuster, 2010). This model explains many features of the tectonic evolution of the Eastern Alps, like the lack of unambiguous remnants of former oceanic material, the high T/P ratio of the rocks, and the short time span of subduction (5–7 Ma; Thöni et al., 2008). However, intracontinental subduction initiation is unconventional (e.g., Stern, 2004) and the forces that trigger this process are unclear. Stüwe and Schuster (2010) suggested that crustal thinning during Permian and subsequent thermal re-equilibration led to a denser-than-average lithosphere in the rift and that the resulting negative buoyancy could have started subduction. These authors also suggested that subduction of the Penninic Ocean was not achieved by a new subduction zone but by the same, initially intracontinental subduction zone, after the Austroalpine continental crust in the lower plate had been completely consumed.

Exhumed HP/UHP rocks are unique proxies allowing reconstruction of the temporal evolution of a subduction zone as well as its thermal structure. In particular, information on the prograde path can be gained by detailed investigation of metamorphic garnets, which are part of the peak-pressure assemblage. Garnets have high affinity

for Lu as well as high $^{176}\text{Lu}/^{177}\text{Hf}$ ratios, which makes them most suitable for precise and accurate Lu-Hf dating of high-grade rocks (e.g., Baxter & Scherer, 2013; Blichert-Toft et al., 1999; Duchêne et al., 1997; Scherer et al., 2000; Smit et al., 2013). In addition, slow rare-earth element (REE) diffusion rates allow garnets to preserve their isotopic compositions at high temperatures; thus, their chemical composition allows attribution to a specific segment of the P-T path (Bloch et al., 2015; Burton et al., 1995; Ganguly et al., 1998; Tirone et al., 2005; van Orman et al., 2002).

The existing petrological and geochronological data from the eclogites of the Austroalpine domain represent a compilation of different approaches and geochronological methods (U-Pb, Sm-Nd, and Lu-Hf). This data does not show if there is a regular relation between location and timing of subduction. In this study we present a coherent, high-precision Lu-Hf data set combined with equilibrium phase diagram modelling, which allows the tectonic environment prevalent during the development of the Austroalpine domain to be constrained. Our results show that the Eoalpine HP belt represents coherent terranes that were progressively subducted and accreted in a short phase (c. 10 Ma) of intracontinental subduction.

2 | REGIONAL GEOLOGY: THE EASTERN ALPS

The Eastern Alps show a complex architecture that was mainly developed during the Cretaceous and Tertiary orogenies. The structurally lower units in the nappe stack are the Penninic nappes. They crop out along the northern margin of the Eastern Alps as well as in the Engadine Window, Tauern Window, and Rechnitz Window (Figure 1). These windows comprise slices of the Piemont-Ligurian Ocean, the Valais Ocean, and the Briançonnais Terrane.

The Austroalpine nappes form the upper part of the nappe stack (Figure 1). They are derived from the continental crust of Apulia (Adria) and are subdivided into Lower and Upper Austroalpine units (Schmid et al., 2004). The Lower Austroalpine units represent the continental margin between Apulia and the Piemont-Ligurian Ocean and occur only locally along the base of the Austroalpine.

The Upper Austroalpine comprises the Northern Calcareous Alps to the north and the Central Austroalpine to the south. The former consists of thick Permo-Mesozoic sediments, the latter of Variscan basement with minor Permo-Mesozoic sedimentary cover. The Northern Calcareous Alps show almost no Alpine metamorphism, whereas parts of the Central Austroalpine have been

metamorphosed up to eclogite-facies conditions (e.g., Frank, 1987; Thöni, 1999).

The Central Austroalpine is further subdivided into (1) Lower Central Austroalpine, which consists of basement largely affected by Cretaceous metamorphism up to eclogite facies and scarce or only locally present Mesozoic sediment cover, and (2) Upper Central Austroalpine comprising low-grade Variscan basement and unmetamorphosed Mesozoic cover remnants (Janák et al., 2004). The Upper Central Austroalpine includes among other units the Northern Grauwacke zone, the Graz Paleozoic, and the Gurktal nappe (Figure 1). The Ötztal-Bundschuh, Koralmpe-Wölz, and Silvretta-Seckau nappe systems of Schmid et al. (2004) form the Lower Central Austroalpine.

Geochronological information for eclogite-facies rocks of the Austroalpine is summarized in Table 1.

2.1 | Variscan HP metamorphism in the Austroalpine

Variscan HP rocks crop out mainly in the western parts of the Austroalpine basement as well as in the Hochgrössen Massif, east of the Tauern Window (Figure 1). U–Pb SHRIMP data for zircons from phengite- and kyanite-bearing eclogites of the Silvretta nappe yielded an age of 351 ± 22 Ma, interpreted to reflect zircon growth during Variscan high-pressure metamorphism (Ladenhauf et al., 2001). Sm–Nd garnet geochronology combined with Rb–Sr dating of mica constrained a similar age for high-pressure imprint in the high-grade rocks of the Ötztal Complex during the Variscan orogeny at c. 350 Ma under P–T conditions of 2.7 GPa and 730°C and Variscan cooling ages at c. 310 Ma (Miller & Thöni, 1995; Neubauer, Hoinkes, et al., 1999; Thöni, 1999). In the Ulten Zone of the Tonale Nappe, south of the Ötztal Complex, Sm–Nd geochronology has been applied to migmatitic gneisses associated with lenses of eclogite and garnet peridotite (Tumiati et al., 2003). Ages of c. 330 Ma were obtained for Variscan high-pressure metamorphism as well as for partial melting, and the entire event was interpreted to represent an episode of crustal subduction at the end of the Variscan orogenic cycle. P–T conditions for the Variscan high-pressure metamorphism were estimated at 1.5 GPa and 600–850°C (Godard et al., 1996).

In metabasites in the Speik Complex (Hochgrössen massif), eclogite-facies conditions were estimated at 1.8–2.2 GPa and 700°C. $^{40}\text{Ar}/^{39}\text{Ar}$ dating of edenitic hornblende in textural equilibrium with omphacite in the eclogites yielded an age of 397.3 ± 7.8 Ma (Faryad

et al., 2002), which is interpreted to be a minimum age for high-pressure metamorphism in the area. This would suggest that the Speik Complex in the Austroalpine basement east of the Tauern Window comprises remnants of the oldest eclogite-facies rocks preserved in the Eastern Alps.

For the eclogites from the Prijakt area in Schobergruppe, Linner (1999) determined HP metamorphic conditions of 1.6–1.8 GPa and 630–690°C. Sm–Nd and Rb–Sr data of eclogites indicate that the Eoalpine pressure peak occurred at c. 115 Ma, followed by amphibolite facies recrystallization before 86 Ma. In contrast, Schulz (1993) interpreted the eclogites to be Variscan. Recently, Hauke et al. (2019) applied Lu–Hf geochronometry on two eclogite samples from the same area. They obtained a minimum age of 313.3 ± 1.8 Ma for one of the samples and a maximum age of 96.92 ± 0.82 Ma for the other sample, showing that the rocks in this area experienced eclogite-facies metamorphism twice, during the Variscan and the Eoalpine cycle. Thermodynamic modelling, performed by the same authors, resulted in Alpine peak pressure conditions of c. 1.9 GPa and 650°C.

2.2 | Alpine HP metamorphism

The Texel complex is the westernmost exposure of high-pressure rocks of the Eoalpine high-pressure belt. HP conditions of 1.2–1.4 GPa and 560–620°C were estimated for the eclogite-facies stage by Hoinkes et al. (1991) and Habler et al. (2006). In contrast, Zanchetta et al. (2013) proposed UHP metamorphic conditions of 2.65–2.90 GPa and 630–690°C, based on high Si-content in matrix phengites as well as K-feldspar and phengite lamellae within omphacite. Dating of the eclogites is rather difficult, because the garnets are inclusion-rich and display two growth stages. Whether or not these growth stages are part of the same metamorphic cycle is still unclear. However, U–Pb zircon dating as well as Sm–Nd garnet dating suggested eclogite-facies metamorphism taking place at 85 ± 4 and 85.2 ± 4.6 Ma, respectively (Habler et al., 2006; Zanchetta, 2007). These results are consistent with Rb–Sr and Ar–Ar mica ages from eclogite host rocks (e.g., Sölva et al., 2001; Thöni, 1983), which indicate that temperatures of $\leq 300^\circ\text{C}$ were reached during cooling close to 70 Ma (Thöni, 1999).

In the northern part of Kreuzeckgruppe further east, Eoalpine eclogites crop out in the cores of large garnet amphibolite bodies (Polinik unit; Hoke, 1990). In a tourmaline-bearing eclogite, Konzett et al. (2012) determined P–T conditions of 2.1 GPa and 650–680°C, as well as U–Pb zircon ages of 86 ± 1 and 109 ± 2 Ma.

TABLE 1 Compilation of geochronological data on (U)HP rocks from the Austroalpine domain

Locality	Lithology	Estimated PT (GPa/°C)	Geochronological method	HP age	Reference
Variscan HP metamorphism					
Silvretta basement	Eclogite	2.8/700	U-Pb SHRIMP	351 ± 22 Ma	Ladenhauf et al. (2001)
Ötztal basement	Eclogite	2.7/730	Sm-Nd	c. 370-340 Ma	Miller and Thöni (1995)
Ulten Zone	Eclogite	1.5/600–850	Sm-Nd	c. 330 Ma	Tumiati et al. (2003)
Speik Complex/Hochgrössen	Eclogite	1.8–2.2/700	Ar-Ar	397.3 ± 7.8 Ma	Faryad et al. (2002)
Schobbergruppe	Eclogite	–	Lu-Hf	313.3 ± 1.8 Ma	Hauke et al. (2019)
Alpine HP metamorphism					
Schobbergruppe	Eclogite	<1.9/630–690	Sm-Nd, Lu-Hf	c. 115 to c. 97	Hauke et al. (2019); Linner (1999)
Texel complex	Eclogite	1.2–1.4/560–620 2.65–2.90/630–690	Sm-Nd, U-Pb	c. 85 Ma	Habler et al. (2006); Hoinkes et al. (1991); Zanchetta (2007)
Kreuzeckgruppe	Eclogite	2.1/650–680	U-Pb	109-86	Konzett et al. (2012)
Saualpe	Eclogite	<2.2/630–740	Sm-Nd, Lu-Hf	94-89	Miller, Thöni, et al. (2005); Thöni and Miller (1996)
Koralpe	Eclogite	2.2–2.5/700–750	Sm-Nd	109-91	Miller and Thöni (1997); Thöni and Jagoutz (1992)
Pohorje	Eclogite, microdiamond-bearing gneiss	≥3.5/800–850	Sm-Nd, Lu-Hf, U-Pb	97-90	Janák et al. (2009, 2015); Miller, Mundil, et al. (2005); Thöni et al. (2008); Sandmann et al. (2016)
Sieggraben	Eclogite	>1.4 to <1.7/>610 to <750	Ar-Ar	136-108	Kromel et al. (2011); Neubauer, Dallmeyer, and Takasu (1999)

In the Koralpe-Saualpe-Pohorje region, Miller (1990) distinguished two different types of eclogites based on geochemical and petrological data: (1) quartz-rich and (2) kyanite-rich eclogites. Both types are derived from N-MORB-type gabbroic protolith of Permian age (Miller & Thöni, 1997; Miller, Thöni, et al., 2005; Thöni & Jagoutz, 1992) but represent different fractionation stages of the igneous source. The quartz-rich eclogites are enriched in FeO and TiO₂ and usually are kyanite-free. They indicate formation from basaltic liquids with normal MORB-affinities. The kyanite-rich eclogites, on the other hand, are characterized by high MgO and Al₂O₃ contents and low TiO₂ contents. They are derived from plagioclase-rich cumulates of the same gabbroic rock-suite.

The polymetamorphic Saualpe Complex comprises eclogites embedded in high-grade paragneisses (e.g., Tenczer & Stüwe, 2003). The Eclogite Unit of

Saualpe is characterized by well-proven Eoalpine eclogite-facies metamorphic imprint. Peak P-T conditions reached up to 2.2 GPa and 630–740°C (Thöni et al., 2008, and references therein). Sm-Nd and Lu-Hf ages obtained from kyanite-bearing and kyanite-free eclogites range between c. 94 and 89–87 Ma (e.g., Miller, 1990; Miller, Thöni, et al., 2005; Thöni et al., 2008; Thöni & Jagoutz, 1992; Thöni & Miller, 1996). The adjacent Koralpe complex is similarly characterized by Eoalpine eclogite-facies rocks. Sm-Nd dating of the eclogites yielded ages between 108.7 ± 8.8 and 91.4 ± 6.7 Ma (Lichem et al., 1997; Miller & Thöni, 1997; Miller, Thöni, et al., 2005; Thöni & Jagoutz, 1992). The estimated peak P-T conditions of 2.2–2.5 GPa and 700–750°C (Miller et al., 2007, and references therein) are similar to those recorded by eclogites from Saualpe.

The Pohorje Mountains comprise the southeasternmost high-grade rocks of the Eoalpine high-

pressure belt. The HP and UHP rocks include eclogites and garnet peridotites (3–4 GPa and 710–940°C; Janák et al., 2004, 2006; Vrabc et al., 2012) as well as microdiamond-bearing gneisses (≥ 3.5 GPa and 800–850°C; M. Janák et al., 2015). A late Cretaceous age for the HP metamorphism has been documented by various geochronological studies. U–Pb zircon dating of eclogites and metapelites yielded ages between c. 93 and c. 90 Ma (Janák et al., 2009; Miller, Mundil, et al., 2005). These ages are identical to the Sm–Nd garnet ages and one Lu–Hf garnet age of eclogites, determined by Miller, Mundil, et al. (2005) and Thöni et al. (2008). Sandmann et al. (2016) obtained ages of 96.6 ± 1.2 and 94.8 ± 5.1 Ma for the eclogites and 91.6 ± 4.1 Ma for the garnet peridotite and interpreted the age results to be related to peak-pressure conditions. Taken together, a clearly documented UHP stage in Pohorje took place between 97 and 90 Ma.

In the north-eastern part of the Austroalpine basement, the Siegraben unit is an eclogite-bearing tectonic mélangé on the border of the Eastern Alps, south of Vienna. Neubauer, Dallmeyer, et al. (1999) estimated peak pressure conditions of 1.4–1.5 GPa and 670–750°C. $^{40}\text{Ar}/^{39}\text{Ar}$ dating of hornblende was conducted by the same authors and yielded ages between c. 136 and 108 Ma. These were interpreted to represent different stages of decompressional retrogression following the HP event (Neubauer, Dallmeyer, et al., 1999). Kromel et al. (2011) defined a new P–T path for the eclogites with peak pressure conditions of 1.6–1.7 GPa and 610–650°C.

For this study, new eclogite samples were collected from Koralpe, Saualpe, Siegraben, and Texel units (Figure 1). The exact coordinates of the sample localities are presented in Table 2.

3 | ANALYTICAL METHODS

Part of the isotopic analyses of Lu and Hf was performed on the ThermoFisher Neptune MC-ICPMS at University of Cologne. All other measurements and analyses were concluded at the Institute of Geosciences, University of Bonn.

3.1 | Bulk and mineral composition analyses

All samples were crushed in a steel mortar. For the whole rock bulk composition analysis representative aliquot of each sample was powdered in an agate mill, and glass beads and pressed pellets were produced for

TABLE 2 Sample locations and GPS coordinates

Location/ Sample	Sample	Coordinates
Koralpe		
Hohl	HO 1 & HO 2	N46°43'49.4" E15°08'48.9"
Saualpe		
Grünburgerbach	GRÜ 1 & GRÜ 2	N46°51'21" E14°34'29.5"
Wolfsberger Hütte	WOL 1	N46°49'60v E14°39'33.5"
Siegraben		
	SIG 3	N47°39'31" E16°21'25"
Texel		
Saltaus Valley	SAL 1	N46°44'07.5" E11°10'32.8"

measurement of major oxides and trace elements, respectively. The X-ray fluorescence analysis was carried out using a PANalytical ProTrace X-ray fluorescence spectrometer. Loss on ignition (L.O.I.) was determined by weight loss before and after heating every sample up to 1,000°C. All the Fe is reported as ferric (Fe^{3+} : Fe_2O_3) in the XRF analysis (Table 3).

For all samples, the major element compositions of minerals as well as the element zoning in garnets were determined by using a JEOL Superprobe JXA 8200 electron microprobe and following the procedure outlined in Miladinova et al. (2018). Two garnet grains were analysed in sample SIG 3; three in HO 1, GRÜ 1, GRÜ 2, and WOL 1; six in HO 2; and nine in sample SAL 1. Trace element distributions in garnets were measured in situ by laser ablation mass spectrometry along line profiles. The analyses were carried out using a Resonetics M50-E ATL Excimer 193 nm laser system coupled to a Thermo X-series 2 quadrupole ICP-MS. The laser was operated using fluency of 7.4 J/cm² at the sample surface and repetition rate of 15 Hz. Different spot sizes were used depending on the grain size of the garnets as well as the distribution of inclusions: 44 and 58 μm . Count rates were normalized using ^{29}Si as an internal standard and NIST-SRM-612 glass as an external standard (Jochum et al., 2011). Reproducibility was checked by measuring the NIST-SRM-610 reference glass and treating it as an unknown. The isotopes ^{43}Ca , ^{47}Ti , ^{55}Mn , ^{89}Y , ^{175}Lu , ^{177}Hf , ^{178}Hf , and ^{180}Hf were monitored. Data reduction and evaluation were carried out following standard procedures (Longerich et al., 1996).

TABLE 3 XRF analyses of the dated eclogite samples, used as input data for thermodynamic modelling

Sample	GRÜ 1	GRÜ 2	HO 1	HO 2	SAL 1	SIG 3	WOL 1
Major oxides (wt %)							
SiO ₂	49.10	49.74	51.47	49.24	49.85	48.39	47.59
Al ₂ O ₃	14.47	14.74	14.76	20.87	13.39	14.18	15.15
Fe ₂ O ₃	11.86	11.15	11.67	4.85	16.50	13.95	12.51
MnO	0.20	0.16	0.18	0.08	0.22	0.30	0.22
MgO	7.99	7.94	7.82	7.39	5.46	6.72	7.18
CaO	10.70	11.22	10.30	13.78	8.49	11.60	12.05
Na ₂ O	3.25	2.60	2.98	1.68	3.17	2.95	2.67
K ₂ O	b.d.	b.d.	0.09	0.01	0.09	0.17	0.09
TiO ₂	1.62	1.55	1.59	0.32	2.50	1.18	1.70
P ₂ O ₅	0.12	0.11	0.12	b.d.	0.25	0.09	0.11
SO ₃	0.01	0.10	0.11	0.09	0.26	0.14	0.06
L.O.I.	1.14	1.10	0.08	1.87	1.05	1.07	1.22
Total sum	100.46	100.41	101.17	100.18	101.23	100.74	100.55
Trace elements (ppm)							
Sc	37.5	31	34.2	23.7	37.7	38.1	30.4
V	327.6	301.7	320.9	133.2	451.1	331.6	331.5
Cr	255.6	256.2	165.6	577.4	248.7	423.7	225.1
Ni	40.6	66	41.6	25	43.4	46	75.4
Cu	69.3	121.8	57.4	77.7	38.7	75.8	175.6
Zn	38.7	84.3	35.4	75.9	26	150.3	32.1
Ga	92.5	58.7	55	31	77.7	154.4	158.3
As	16.4	16	15.6	13.6	19.8	15.2	16.5
Rb	5.1	1.7	1.4	1.9	3	b.d.	2.4
Sr	1	1.5	3.1	1.8	b.d.	3.3	3.5
Y	42.5	128.5	100.4	156.4	72.9	223.7	144.5
Zr	33.7	30.9	34.1	7.9	58.6	27.4	36.5
Nb	89.1	81.2	102.2	6.4	181.1	66.1	99.8
Mo	2.2	2.4	2.1	b.d.	11	2.6	3.9
Cs	3.2	2.4	b.d.	3.9	8.3	1.2	1.5
Ba	4.4	b.d.	b.d.	4.2	b.d.	2.1	b.d.
La	b.d.	2.8	11.8	49.4	11.1	18.6	5.8
Ce	48.5	37.8	49.5	b.d.	82.9	32	58.7
Nd	16.2	5.1	16.4	10.7	35.1	14.6	9.9
Sm	4	1.7	6.3	6.4	24.2	6.3	5
Hf	b.d.	b.d.	b.d.	b.d.	10.5	1.3	3.9
W	2.1	3.5	3.2	b.d.	3.6	b.d.	3.2
Pb	32.9	68.1	36.3	14.5	54.1	45.5	58.7
Th	11.5	15.2	11.7	16	11.4	8.8	18.6
U	b.d.	b.d.	b.d.	b.d.	2.8	1.2	2.1

3.2 | Lu-Hf dating

The samples selected for Lu-Hf dating were crushed in a steel mortar. One portion of every sample was powdered in an agate mill for bulk rock analysis. For mineral separation, a second portion of every sample was sieved, and the target fractions were then purified using a Frantz magnetic separator. Subsequently, garnet and omphacite were hand-picked under a binocular microscope from 180–255, 250–355, and 355–500 μm size fractions.

Sample digestion was conducted as described in detail by Miladinova et al. (2018). For a complete sample digestion, one whole rock powder split of each sample was digested inside steel-jacketed PARR bombs. The mineral separates and a second whole rock fraction from each sample were dissolved following the selective tabletop procedure described by Lagos et al. (2007). This method avoids digestion of refractory Hf-rich phases like zircon and rutile. The single-column element separation procedure (Münker et al., 2001) was used to separate Lu and Hf from the rock matrix. In addition, the Hf cuts were processed a second time in order to remove the remaining matrix elements Lu and Yb.

The isotopic analyses of Lu and Hf were carried out in static mode using a Thermo-Finnigan Neptune MC-ICP-MS. Measured Hf isotope ratios were corrected for mass fractionation using the exponential law and a $^{179}\text{Hf}/^{177}\text{Hf}$ of 0.7325. All measured $^{176}\text{Hf}/^{177}\text{Hf}$ ratios are reported relative to $^{176}\text{Hf}/^{177}\text{Hf} = 0.282160$ for the Münster Ames Hf standard, which is isotopically identical to the JMC-475 standard. Interferences on ^{176}Hf and ^{180}Hf were corrected by monitoring ^{173}Yb , ^{175}Lu , ^{181}Ta , and ^{182}W signals. The $^{176}\text{Hf}/^{177}\text{Hf}$ was calculated using both the spiked and natural $^{175}\text{Lu}/^{176}\text{Lu}$ composition for interference correction, and the mean $^{176}\text{Hf}/^{177}\text{Hf}$ was used. The respective uncertainty was added to the 2σ external reproducibility in $^{176}\text{Hf}/^{177}\text{Hf}$ that was calculated via an empirical relationship (Bizzaro et al., 2003). The 2s.d. reproducibility of solution standards within the single analytical sessions was ± 0.000029 ($n = 14$, 1.4 V avg. ^{177}Hf signal; mean $^{176}\text{Hf}/^{177}\text{Hf} = 0.282167$) for the $^{176}\text{Hf}/^{177}\text{Hf}$ of the in-house AMES Hf standard analysed at 4–40 ppb Hf. Isochron regressions and ages were obtained using the Isoplot v. 2.49 program of Ludwig (2001) and the ^{176}Lu decay constant $\lambda = 1.867 \times 10^{-11} \text{ yr}^{-1}$ (Scherer et al., 2001; Söderlund et al., 2004) as well as 2σ uncertainties for $^{176}\text{Lu}/^{177}\text{Hf}$ and $^{176}\text{Hf}/^{177}\text{Hf}$ ratios. Total procedural blanks were typically <58 pg for Lu and <64 pg for Hf.

4 | RESULTS

4.1 | Petrography and mineral chemistry

Representative microprobe analyses of minerals from the investigated samples are listed in Table 4.

4.1.1 | Koralpe

Sample HO 1: Quartz-rich eclogite, Hohl

Sample HO 1 is a medium- to coarse-grained eclogite composed of garnet, clinopyroxene, clinozoisite, amphibole, and quartz. Accessory rutile, ilmenite, and apatite are also present. Retrogression is locally restricted and documented by symplectites of Na-poor clinopyroxene, calcic amphibole, and sodic plagioclase around omphacite (Figure 2a). Garnet crystals are anhedral and reach up to 1.5 mm in size. Usually, garnet cores contain inclusions of quartz, rutile, and apatite but may also be inclusion-free. High-resolution X-ray maps reveal rather homogenous grains with respect to bivalent cations, but some patches show slightly different compositions enriched in Mn and Fe (Figure 3). In contrast to the largely equilibrated major elements, Lu concentration profiles display a well-developed bell-shaped distribution (Figure 3). Omphacite occurs as large anhedral crystals in the matrix and is unzoned. The molar fraction of jadeite in omphacite is 0.39–0.42. Locally, diopside-rich clinopyroxene ($X_{\text{Jd}} = 0.12$) together with Na-rich plagioclase (An_{14-17}) and calcic amphibole form symplectitic rims around omphacite. Amphibole is a minor phase and occurs as single grains or in symplectites replacing omphacite. Both varieties have pargasitic composition with Al_2O_3 contents varying between 13.17 and 14.08 wt % and Na_2O of 3.47–3.89 wt%.

Sample HO 2: Kyanite-rich eclogite, Hohl

The mineral composition of this eclogite reflects its Mg- and Al-rich bulk composition. It contains Mg-rich garnet, omphacite, clinozoisite, kyanite, quartz, amphibole, and rutile (Figure 2c,d). Retrogressive alteration is limited and restricted to narrow symplectite rims around omphacite, which consist of Na-poor clinopyroxene + sodic plagioclase \pm calcic amphibole. The garnets are poikiloblastic with inclusions of omphacite, kyanite, amphibole, clinozoisite, quartz, and minor rutile in the cores, whereas the rims are inclusion-free. The chemical composition of the garnets is nearly constant with little variation in content of the major elements ($\text{Prp}_{39-42}\text{Alm}_{34-37}\text{Grs}_{22-25}\text{Sps}_{0.4-0.8}$), which is also illustrated by the compositional maps (Figure 4). Unzoned omphacite with jadeite content between 25% and 30%

TABLE 4 Representative microprobe analyses of eclogite minerals in wt% and p.f.u.

Sample	HO 1	HO 1	HO 1	HO 1	HO 1	HO 1	HO 1	HO 1	HO 1	HO 2	HO 2	HO 2	HO 2	HO 2	HO 2	HO 2	HO 2	HO 2	HO 2	GRÜ 1	GRÜ 1
Mineral	Grt rim	Grt core	Grt	Omp/mtx	Cps/syml	Am	Pl	HO 1	HO 1	Grt rim	Grt core	Omp/mtx	Cps/syml	Am	Ep/Czo	Pl	Ky	HO 2	HO 2	GRÜ 1	GRÜ 1
SiO ₂	39.25	39.07	55.06	53.46	43.58	65.26	40.16	39.86	54.84	52.92	46.37	39.09	63.40	36.80	38.50					40.94	38.50
TiO ₂	0.05	0.06	0.09	0.04	0.73	0.00	0.05	0.05	0.15	0.10	0.62	0.05	0.06	0.06	0.07					0.07	0.07
Al ₂ O ₃	21.46	21.43	10.56	2.19	13.17	22.19	22.94	22.94	8.63	5.79	15.29	32.32	23.08	62.25	21.95					19.35	21.95
FeO/Fe ₂ O ₃	22.70	21.97	5.21	9.01	13.19	0.18	16.94	16.13	2.54	3.72	6.42	1.29	0.06	0.61	21.55					21.25	21.55
MnO	0.25	0.46	0.04	0.09	0.06	0.01	0.22	0.21	0.01	0.01	0.06	0.01	0.00	0.00	0.32					0.26	0.32
MgO	7.37	6.41	8.92	12.15	12.67	0.00	11.37	11.01	11.98	13.63	15.36	0.07	0.01	0.00	7.40					9.10	7.40
CaO	8.51	10.05	14.38	20.88	10.42	2.64	8.22	8.98	18.57	21.97	10.99	23.82	4.24	0.05	9.60					8.29	9.60
Na ₂ O	0.06	0.07	6.08	1.97	3.47	10.19	0.01	0.05	3.94	1.82	2.63	0.00	9.34	0.00	0.06					0.02	0.06
K ₂ O	0.01	0.01	0.01	0.00	0.41	0.03	0.01	0.00	0.01	0.00	0.20	0.00	0.08	0.01	0.03					0.01	0.03
Cr ₂ O ₃	0.06	0.03	0.00	0.04	0.01	0.04	0.08	0.01	0.11	0.06	0.07	0.04	0.00	0.02	0.00					0.01	0.00
Sum	99.70	99.55	100.34	99.84	97.71	100.54	100.00	99.23	100.77	100.02	98.00	96.68	100.26	99.79	99.48					99.29	99.48
Si	6.04	6.04	1.97	1.99	6.38	2.86	5.98	5.98	1.95	1.92	6.50	3.01	2.80	3.99	5.94					6.27	5.94
Ti	0.01	0.01	0.00	0.00	0.08	0.00	0.01	0.01	0.00	0.00	0.07	0.00	0.00	0.00	0.01					0.01	0.01
Al	3.89	3.90	0.44	0.10	2.27	1.15	4.03	4.05	0.36	0.25	2.53	2.93	1.20	7.96	3.99					3.49	3.99
Fe	2.92	2.84	0.16	0.28	1.62	0.01	2.11	2.02	0.08	0.11	0.75	0.07	0.00	0.06	2.78					2.72	2.78
Mn	0.03	0.06	0.00	0.00	0.01	0.00	0.03	0.03	0.00	0.00	0.01	0.00	0.00	0.00	0.04					0.03	0.04
Mg	1.69	1.48	0.47	0.68	2.77	0.00	2.52	2.46	0.63	0.74	3.21	0.01	0.00	0.00	1.70					2.08	1.70
Ca	1.40	1.66	0.55	0.83	1.64	0.12	1.31	1.44	0.71	0.86	1.65	1.96	0.20	1.36	1.59					1.36	1.59
Na	0.02	0.02	0.42	0.14	0.99	0.87	0.00	0.01	0.27	0.13	0.71	0.00	0.80	0.00	0.02					0.01	0.02
K	0.00	0.00	0.00	0.00	0.08	0.00	0.00	0.00	0.00	0.00	0.04	0.00	0.00	0.00	0.01					0.00	0.01
Cr	0.01	0.00	0.00	0.00	0.00	0.00	0.01	0.00	0.00	0.00	0.01	0.00	0.00	0.00	0.00					0.00	0.00
Sum	16.01	16.01	4.02	4.03	15.82	5.00	16.00	16.00	4.00	4.01	15.47	7.99	5.00	12.02	16.07					15.98	16.07
O	24.00	24.00	6.00	6.00	23.00	8.00	24.00	24.00	6.00	6.00	23.00	12.50	8.00	20.00	24.00					24.00	24.00
Xalm	0.48	0.47	-	-	-	-	0.35	0.34	-	-	-	-	-	-	0.46					0.44	0.46
Xgrs	0.23	0.28	-	-	-	-	0.22	0.24	-	-	-	-	-	-	0.26					0.22	0.26
Xprp	0.28	0.24	-	-	-	-	0.42	0.41	-	-	-	-	-	-	0.28					0.34	0.28
Xjd	-	-	0.41	0.11	-	-	-	-	0.29	0.15	-	-	-	-	-					-	-

Note: Fe is calculated as Fe²⁺, except for epidote/clinozoisite where Fe is Fe³⁺.

TABLE 4 (Continued)

Sample	GRÜ1		GRÜ2		GRÜ2		GRÜ2		GRÜ2		GRÜ2		WOL1		WOL1		WOL1		WOL1		
Mineral	Omp/mtx	Cps/syml	Am	Pl	Grt rim	Grt core	Omp/mtx	Am	Pl	Ep/Czo	Grt rim	Grt core	Omp/mtx	Am	Pl	Cpx/syml	Omp/mtx	Am	Pl	Ep/Czo	
SiO ₂	54.12	52.25	43.38	63.80	39.53	39.45	54.97	46.16	63.38	39.65	39.03	38.36	55.65	43.63	64.72	54.16	55.65	43.63	64.72	40.06	40.06
TiO ₂	0.18	0.22	0.57	0.00	0.01	0.10	0.13	0.86	0.00	0.04	0.02	0.12	0.13	0.80	0.04	0.19	0.13	0.80	0.04	0.08	0.08
Al ₂ O ₃	11.10	7.84	16.67	23.51	22.64	22.31	10.05	13.96	23.04	31.09	21.96	21.81	10.31	14.15	21.77	4.58	10.31	14.15	21.77	32.19	32.19
FeO/ Fe ₂ O ₃	4.48	5.55	0.02	0.20	20.42	20.64	3.88	8.68	0.07	2.17	22.66	23.02	3.76	11.63	0.11	4.96	3.76	11.63	0.11	1.25	1.25
MnO	0.00	0.01	0.01	0.03	0.19	0.37	0.00	0.11	0.00	0.00	0.22	0.40	0.00	0.09	0.03	0.04	0.00	0.09	0.03	0.01	0.01
MgO	9.05	11.34	10.79	0.01	9.41	8.22	9.67	13.92	0.01	0.05	6.51	4.05	9.75	12.55	0.01	13.16	9.75	12.55	0.01	0.04	0.04
CaO	14.91	19.71	12.34	3.75	8.34	9.56	15.53	10.00	3.59	24.15	9.64	11.98	15.77	11.11	3.22	21.29	15.77	11.11	3.22	24.09	24.09
Na ₂ O	5.73	3.05	9.64	9.81	0.03	0.01	5.25	3.48	9.98	0.05	0.03	0.00	5.34	3.32	10.32	2.08	5.34	3.32	10.32	0.01	0.01
K ₂ O	0.01	0.00	4.17	0.03	0.00	0.01	0.00	0.13	0.00	0.01	0.00	0.01	0.00	0.23	0.02	0.00	0.00	0.23	0.02	0.01	0.01
Cr ₂ O ₃	0.06	0.03	0.14	0.01	0.00	0.06	0.03	0.04	0.02	0.05	0.05	0.07	0.08	0.06	0.04	0.04	0.08	0.06	0.04	0.02	0.02
Sum	99.63	100.00	97.74	101.15	100.58	100.73	99.50	97.33	100.10	97.26	100.11	99.80	100.79	97.55	100.28	100.49	100.79	97.55	100.28	97.77	97.77
Si	1.94	1.91	6.25	2.79	5.95	5.97	1.97	6.60	2.80	3.05	6.00	5.98	1.97	6.37	2.85	1.97	1.97	6.37	2.85	3.04	3.04
Ti	0.00	0.01	0.06	0.00	0.00	0.01	0.00	0.09	0.00	0.00	0.00	0.01	0.00	0.09	0.00	0.01	0.00	0.09	0.00	0.00	0.00
Al	0.47	0.34	2.83	1.21	4.02	3.98	0.42	2.35	1.20	2.81	3.98	4.01	0.43	2.43	1.13	0.20	0.43	2.43	1.13	2.88	2.88
Fe	0.13	0.17	1.20	0.01	2.57	2.61	0.12	1.04	0.00	0.13	2.91	3.00	0.11	1.42	0.00	0.15	0.11	1.42	0.00	0.07	0.07
Mn	0.00	0.00	0.00	0.00	0.02	0.05	0.00	0.01	0.00	0.00	0.03	0.05	0.00	0.01	0.00	0.00	0.00	0.01	0.00	0.00	0.00
Mg	0.48	0.62	2.65	0.00	2.11	1.85	0.52	2.96	0.00	0.01	1.49	0.94	0.51	2.73	0.00	0.71	0.51	2.73	0.00	0.00	0.00
Ca	0.57	0.77	1.49	0.18	1.35	1.55	0.60	1.53	0.17	1.99	1.59	2.00	0.60	1.74	0.15	0.83	0.60	1.74	0.15	1.96	1.96
Na	0.40	0.22	1.20	0.83	0.01	0.00	0.37	0.96	0.85	0.01	0.01	0.00	0.37	0.94	0.88	0.15	0.37	0.94	0.88	0.00	0.00
K	0.00	0.00	0.03	0.00	0.00	0.00	0.00	0.02	0.00	0.00	0.00	0.00	0.00	0.04	0.00	0.00	0.00	0.04	0.00	0.00	0.00
Cr	0.00	0.00	0.00	0.00	0.00	0.01	0.00	0.00	0.00	-	0.01	0.01	0.00	0.01	0.00	0.00	0.00	0.01	0.00	-	-
Sum	4.01	4.03	15.72	5.02	16.04	16.03	4.00	15.58	5.03	7.99	16.01	16.00	3.99	15.77	5.02	4.00	3.99	15.77	5.02	7.97	7.97
O	6.00	6.00	23.00	8.00	24.00	24.00	6.00	23.00	8.00	12.50	24.00	24.00	6.00	23.00	8.00	6.00	6.00	23.00	8.00	12.50	12.50
Xalm	-	-	-	-	0.43	0.43	-	-	-	-	0.48	0.50	-	-	-	-	-	-	-	-	-
Xgrs	-	-	-	-	0.22	0.26	-	-	-	-	0.26	0.33	-	-	-	-	-	-	-	-	-
Xprp	-	-	-	-	0.35	-	-	-	-	-	0.25	0.16	-	-	-	-	-	-	-	-	-
Xjd	0.41	0.22	-	-	-	-	0.38	-	-	-	-	-	0.39	-	-	0.15	-	-	-	-	-

TABLE 4 (Continued)

Sample	SIG 3		SIG 3		SIG 3		SIG 3		SIG 3		SIG 3		SIG 3		SAL 1		SAL 1		SAL 1		SAL 1		
	Grt rim	Grt core	Omp/mtx	Cpx/syntl	Am	Pl	Kfs	Ep/Czo	Grtl rim	Grtl core	Grt2	Omp/mtx	Cpx/syntl	Am	Pl	SAL 1	SAL 1	SAL 1	SAL 1	SAL 1	SAL 1	Ep/Czo	
SiO ₂	38.13	38.35	51.68	51.66	42.29	65.48	62.84	38.53	36.87	39.23	37.44	55.48	52.30	44.72	67.25	38.16							
TiO ₂	0.08	0.25	0.19	0.11	0.84	0.02	0.04	0.16	0.08	0.05	0.03	0.14	0.08	0.63	0.00	0.14							
Al ₂ O ₃	22.01	21.64	6.61	3.43	13.09	22.07	18.34	27.69	21.90	21.19	21.61	10.36	4.24	12.42	20.40	26.66							
FeO/Fe ₂ O ₃	24.43	22.70	9.78	10.14	16.55	0.09	0.65	8.46	28.97	25.76	25.31	6.73	8.68	15.45	0.36	9.59							
MnO	0.22	1.65	0.09	0.07	0.06	0.00	0.05	0.03	0.41	0.42	0.37	0.01	0.00	0.04	0.02	0.03							
MgO	5.00	3.09	8.84	11.10	10.19	0.01	0.00	0.12	4.85	2.73	3.75	7.31	11.12	11.00	0.02	0.08							
CaO	9.74	11.75	18.22	20.82	11.90	2.64	0.06	23.60	5.48	11.28	9.79	12.09	18.89	7.91	1.13	22.09							
Na ₂ O	0.01	0.03	3.37	1.83	2.59	9.39	0.43	0.00	0.05	0.07	0.05	7.58	3.15	4.52	11.00	0.01							
K ₂ O	0.02	0.01	0.00	0.01	0.36	0.08	16.17	0.00	0.00	0.03	0.02	0.02	0.01	0.55	0.03	0.00							
Cr ₂ O ₃	0.11	0.00	0.00	0.00	0.08	0.03	0.00	0.04	0.01	0.00	0.01	0.02	0.07	0.00	0.00	0.00							
Sum	99.74	99.47	98.77	99.16	97.93	99.80	98.59	98.63	98.61	100.75	98.37	99.74	98.53	97.23	100.21	96.75							
Si	5.95	6.02	1.94	1.95	6.32	2.88	2.97	2.99	5.89	6.11	5.96	2.00	1.97	6.60	2.94	3.01							
Ti	0.01	0.03	0.01	0.00	0.09	0.00	0.00	0.01	0.01	0.01	0.00	0.00	0.00	0.07	0.00	0.01							
Al	4.04	4.00	0.29	0.15	2.30	1.14	1.02	2.53	4.12	3.89	4.06	0.44	0.19	2.16	1.05	2.48							
Fe	3.18	2.98	0.31	0.32	2.07	0.00	0.03	0.49	3.87	3.35	3.37	0.20	0.27	1.91	0.01	0.57							
Mn	0.03	0.22	0.00	0.00	0.01	0.00	0.00	0.00	0.06	0.05	0.05	0.00	0.00	0.01	0.00	0.00							
Mg	1.16	0.72	0.50	0.63	2.27	0.00	0.00	0.01	1.15	0.63	0.89	0.39	0.62	2.42	0.00	0.01							
Ca	1.63	1.98	0.73	0.84	1.90	0.12	0.00	1.96	0.94	1.88	1.67	0.47	0.76	1.25	0.05	1.87							
Na	0.00	0.01	0.25	0.13	0.75	0.80	0.04	0.00	0.02	0.02	0.01	0.53	0.23	1.29	0.93	0.00							
K	0.00	0.00	0.00	0.00	0.07	0.00	0.97	0.00	0.00	0.00	0.00	0.00	0.00	0.10	0.00	0.00							
Cr	0.01	0.00	0.00	0.00	0.01	0.00	0.00	-	0.00	0.00	0.00	0.00	0.00	0.00	0.00	0.00							
Sum	16.02	15.96	4.03	4.03	15.78	4.95	5.03	7.99	16.05	15.95	16.02	4.04	4.05	15.81	5.00	7.95							
O	24.00	24.00	6.00	6.00	23.00	8.00	8.00	12.50	24.00	24.00	24.00	6.00	6.00	23.00	8.00	12.50							
Xalm	0.53	0.51	-	-	-	-	-	-	0.64	0.57	0.56	-	-	-	-	-							
Xgrs	0.27	0.34	-	-	-	-	-	-	0.16	0.32	0.28	-	-	-	-	-							
Xprp	0.19	0.12	-	-	-	-	-	-	0.19	0.11	0.15	-	-	-	-	-							
Xjd	-	-	0.24	0.12	-	-	-	-	-	-	-	0.48	0.19	-	-	-							

Note: Fe is calculated as Fe²⁺, except for epidote/clinozoisite where Fe is Fe³⁺.

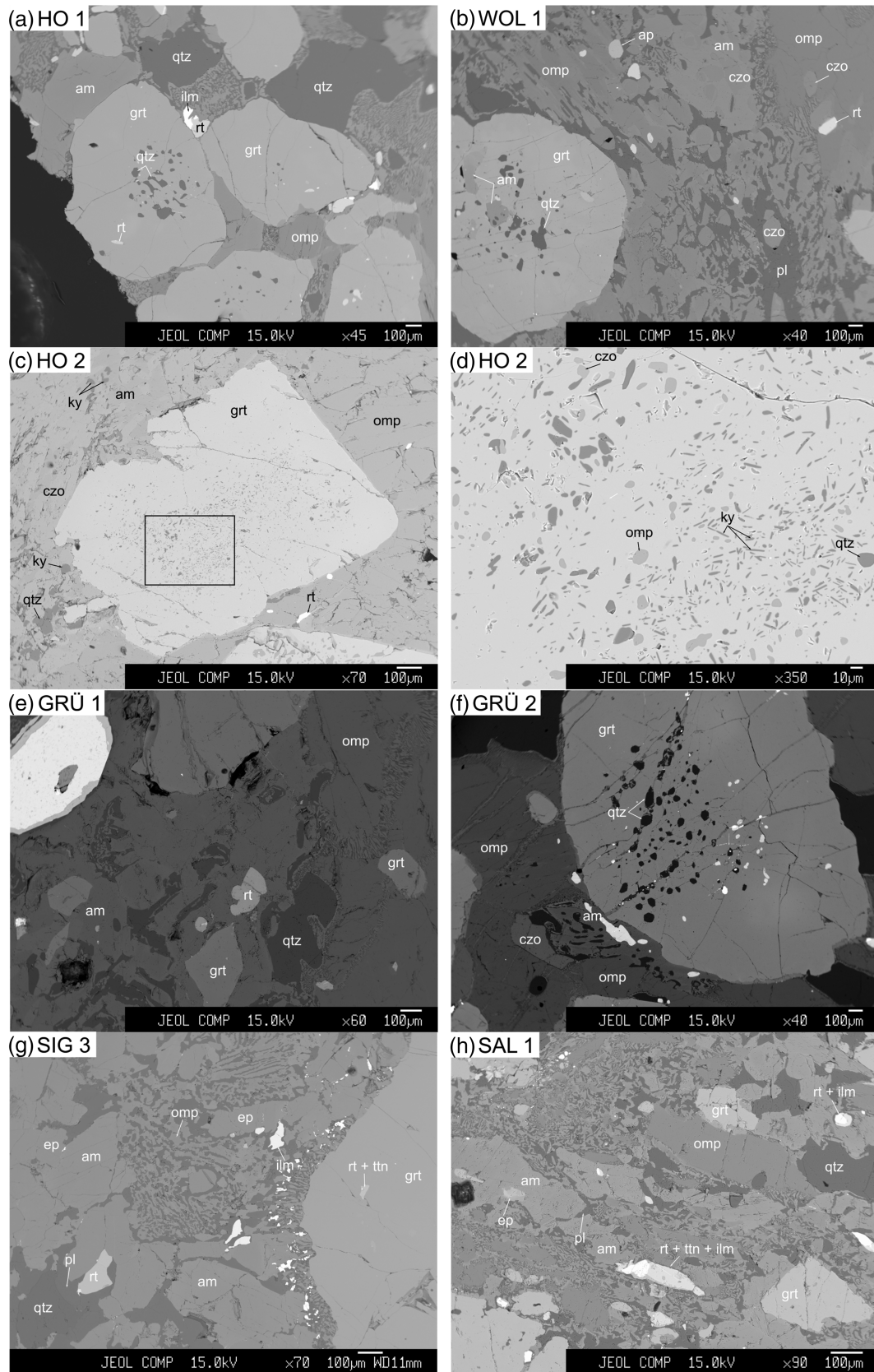


FIGURE 2 Back-scattered electron (BSE) images showing the matrix compositions of the dated eclogite samples. *am*, amphibole; *ap*, apatite; *czo*, clinozoisite; *ep*, epidote; *grt*, garnet; *ilm*, ilmenite; *ky*, kyanite; *omp*, omphacite; *pl*, plagioclase; *qtz*, quartz; *rt*, rutile; *ttn*, titanite

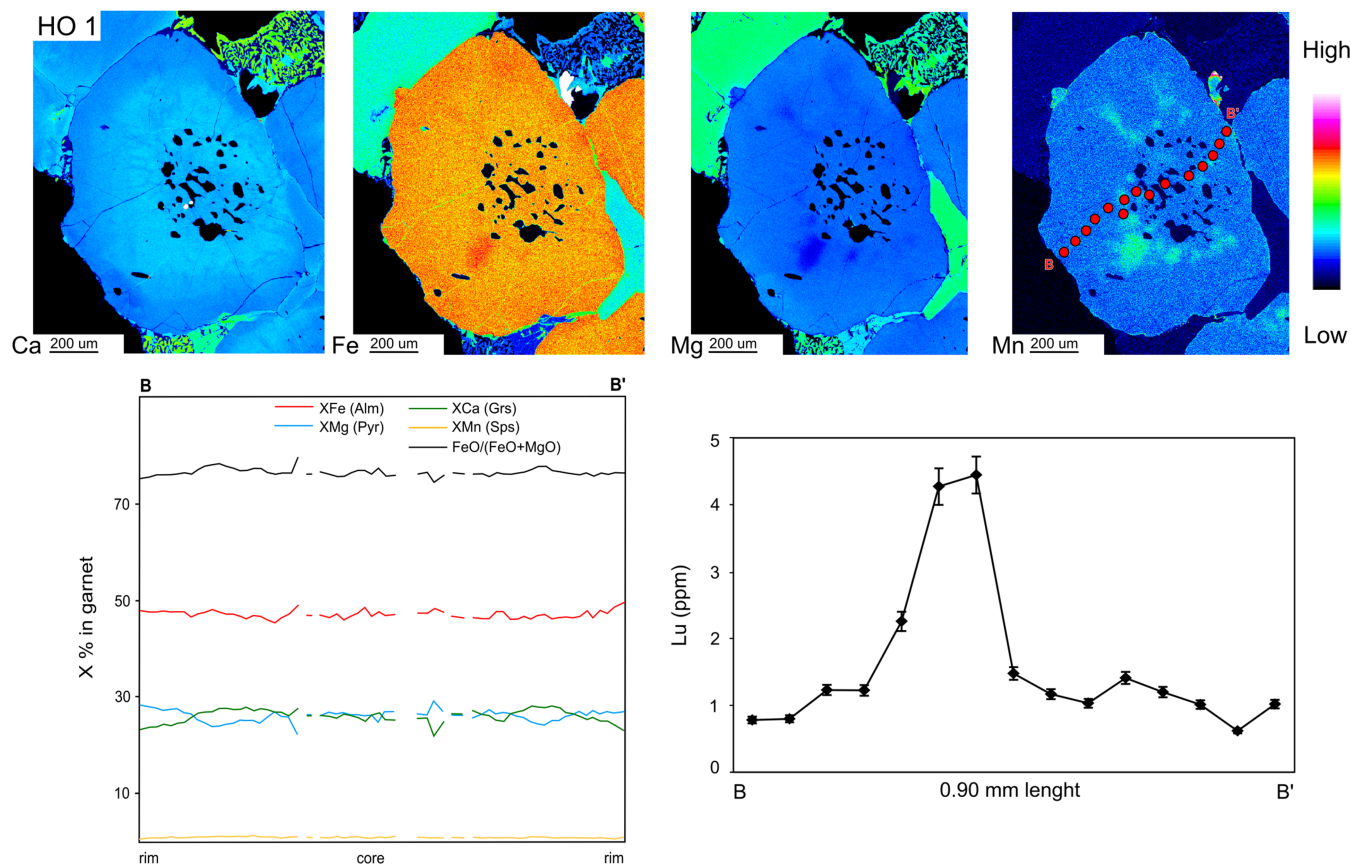


FIGURE 3 Major element distribution maps of a representative garnet of sample HO 1. Compositional and Lu concentration profiles follow the trace B-B' indicated on the map. The bell-shaped pattern of Lu shows preserved prograde growth zonation [Color figure can be viewed at wileyonlinelibrary.com]

occurs as single crystals in the matrix. Omphacite inclusions in garnet and quartz have the same composition as matrix omphacite. Clinopyroxene in symplectites replacing omphacite is Na-poorer with varying jadeite component up to 18%. Amphibole occurs in the matrix and as inclusions in garnet. According to the classification of Hawthorne et al. (2012), the matrix amphibole is magnesio-hornblende with Al_2O_3 content ranging between 12.92 and 15.29 wt%. Pargasite is characterized by Al_2O_3 content of 13.08–13.92 wt%. It occurs as inclusions in garnet and commonly replaces omphacite in symplectites together with diopside and plagioclase. Kelyphitic amphibole replacing garnet at the rims displays very Al-rich composition with Al_2O_3 up to 21 wt% and is classified as sadanagaite (Hawthorne et al., 2012). Clinzoisite with Fe_2O_3 content varying from 1.14 to 1.95 wt% occurs in textural equilibrium with omphacite and amphibole in the matrix. Clinzoisite enclosed by garnet has the same composition. Kyanite is unaltered and occurs as prismatic, subhedral crystals in the matrix. It is compositionally homogenous and contains 0.02–0.12 wt% Cr_2O_3 and 0.18–0.34 wt% Fe_2O_3 as main impurities. Numerous small needles of kyanite enclosed by garnet can contain up to 1.02 wt% Fe_2O_3 .

4.1.2 | Saualpe

Samples GRÜ 1 & GRÜ 2: Quartz-rich eclogite, Grünburger Bach

The eclogite from Grünburger Bach is coarse-grained and made up of garnet, omphacite, clinzoisite, quartz, rutile, and apatite (Figure 2e,f). Weak retrogression is indicated by the breakdown of omphacite to symplectites composed of Na-poor clinopyroxene, sodic plagioclase, and calcic amphibole. Garnet crystals are anhedral to subhedral and reach up to 2.5 mm in size. Garnet is almandine-rich and contains inclusions of quartz and rutile. X-ray maps of major elements as well as compositional profiles show typical prograde zoning with high spessartine and grossular components in the core, whereas the pyrope component is increasing toward the rims (Figures 5 and 6). Lu distribution through garnet shows a bell-shaped pattern. Omphacite is present as relatively large anhedral crystals in the matrix. It contains 36% to 41% jadeite in addition to 1–6% acmite. It contains inclusions of rutile, apatite, and quartz and is variably replaced by diopside-rich clinopyroxene (Jd_8) together with albite-rich plagioclase (An_{20}) and pargasitic amphibole. Clinzoisite is

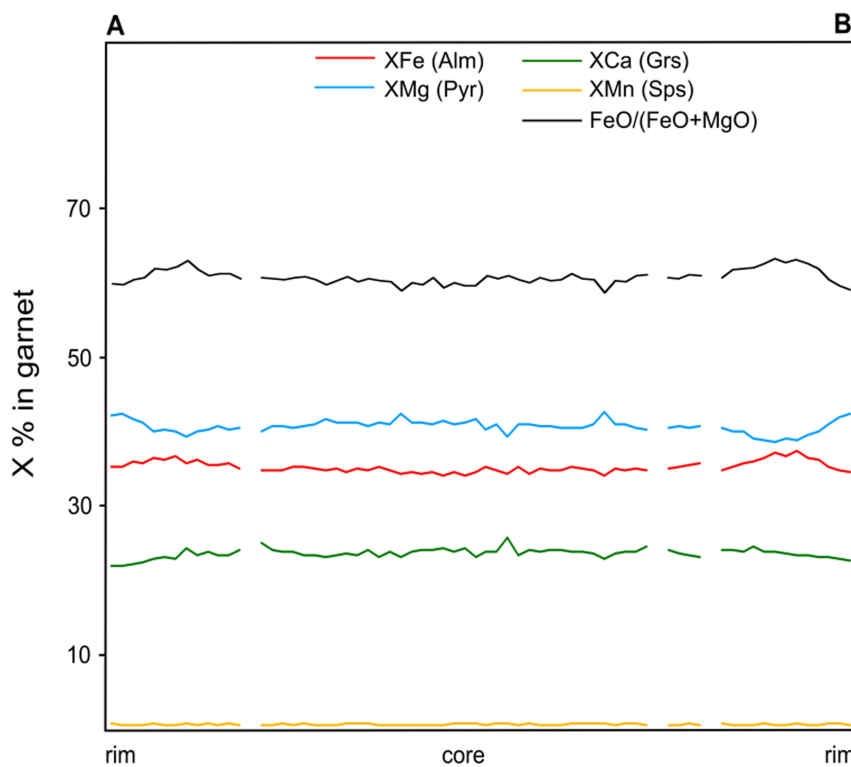
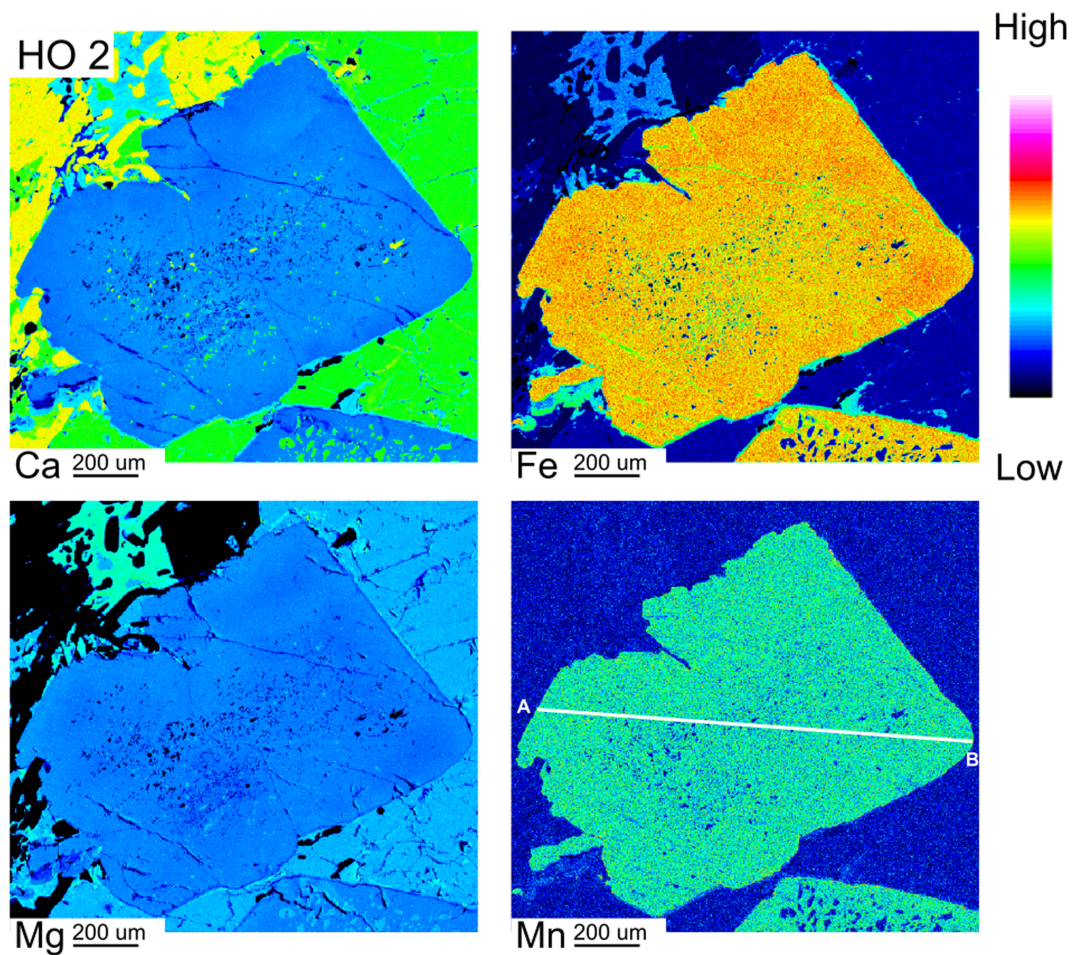


FIGURE 4 Major element distribution maps of a representative garnet of sample HO 2. Compositional profiles follow the line A-B indicated on the map. Maps and profile show homogenized element distribution related to equilibrium during the thermal stage of metamorphism [Color figure can be viewed at wileyonlinelibrary.com]

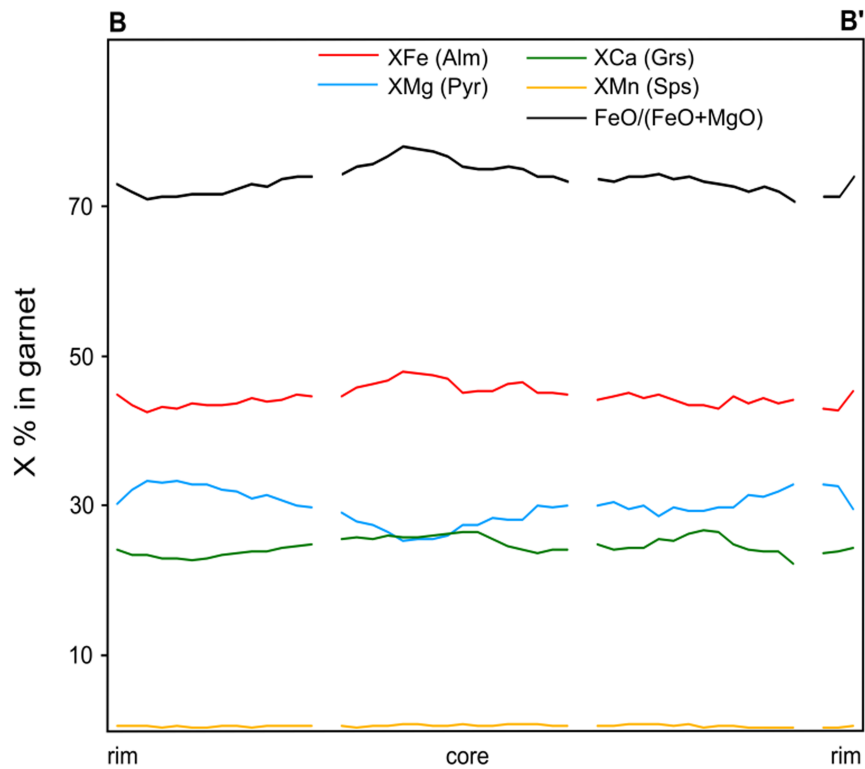
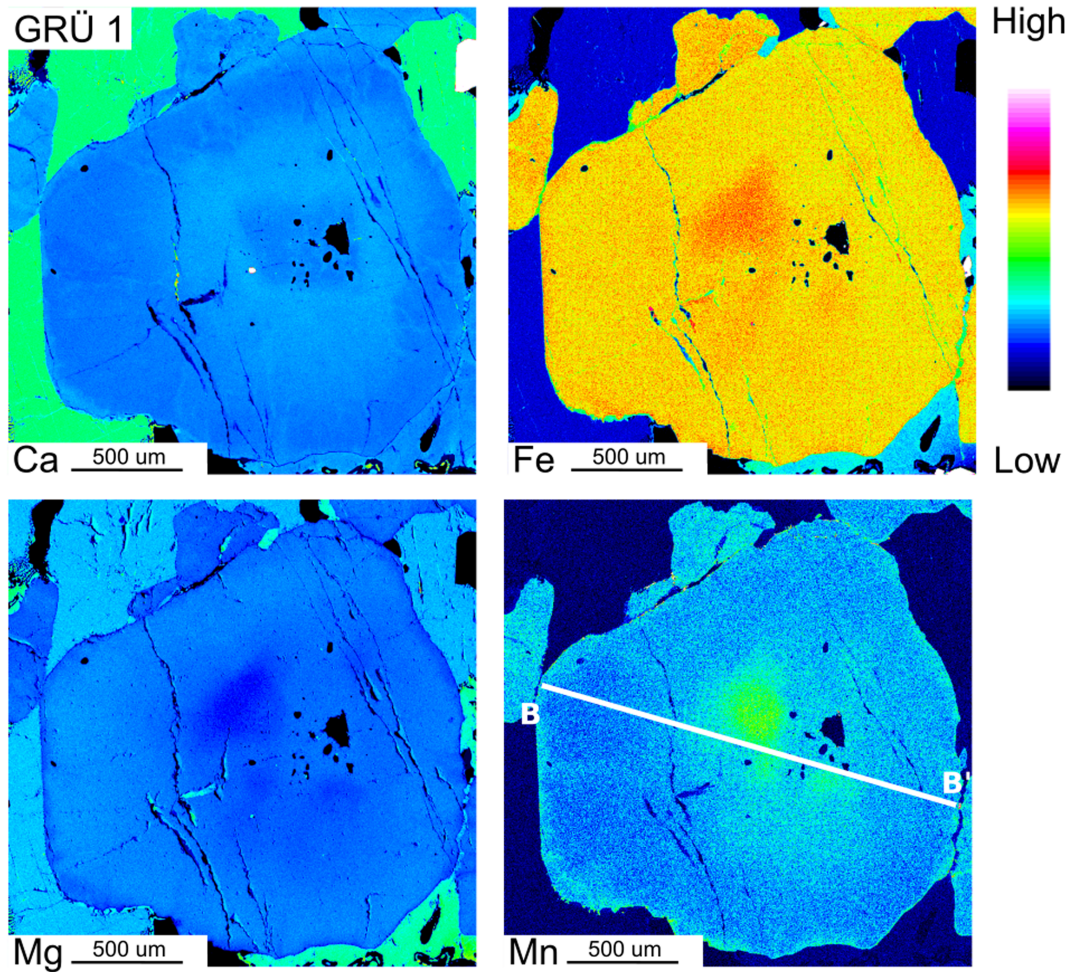


FIGURE 5 Major element distribution maps of a representative garnet of sample GRÜ 1. Compositional profiles in garnet show bell-shaped distribution indicating prograde garnet growth [Color figure can be viewed at wileyonlinelibrary.com]

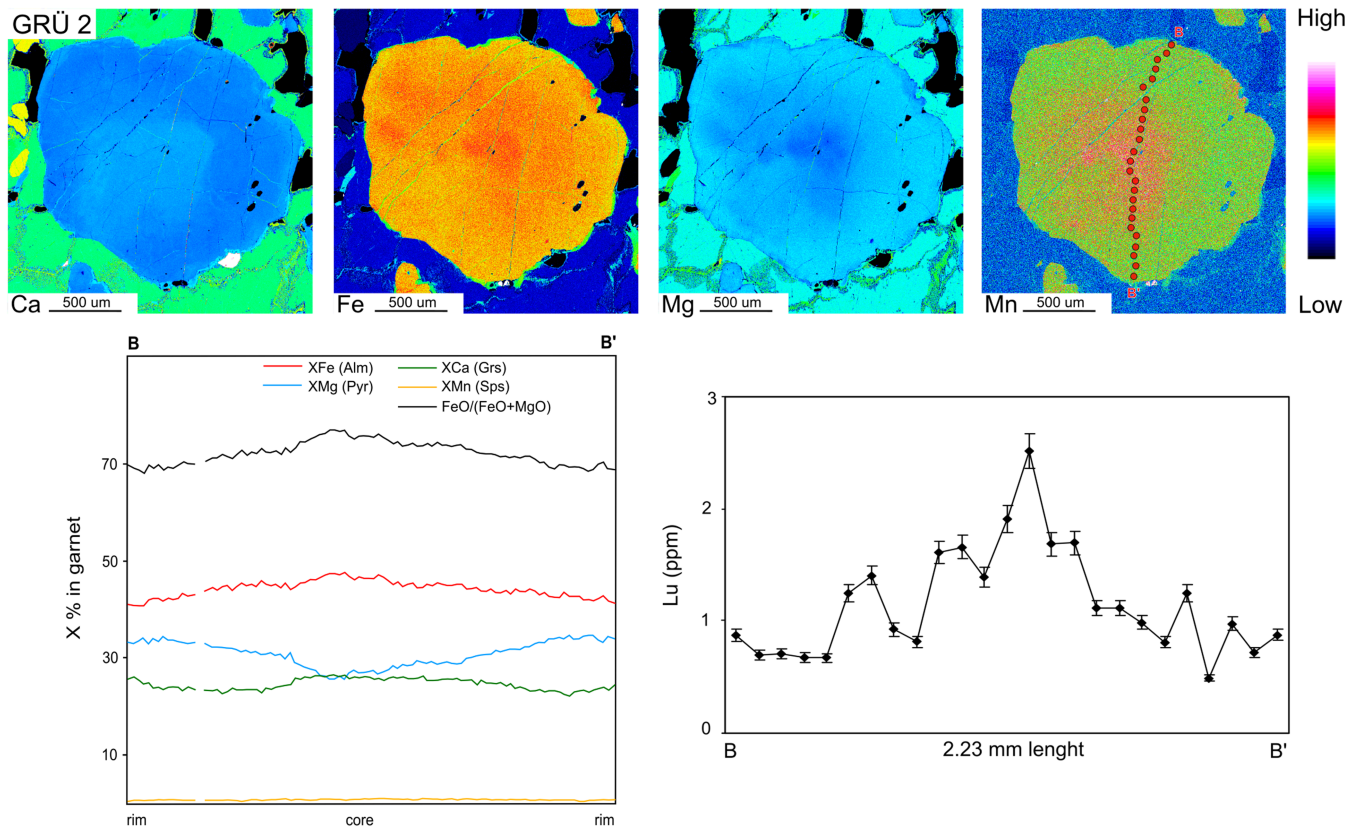


FIGURE 6 Major element distribution maps of a representative garnet of sample GRÜ 2. Compositional profiles as well as Lu concentration profile show bell-shaped distribution indicating prograde garnet growth [Color figure can be viewed at wileyonlinelibrary.com]

abundant in the matrix and forms medium to small grains with relatively low Fe_2O_3 content (2.02–2.63 wt %). Amphibole forms poikiloblasts with pargasitic composition. It also occurs in narrow symplectite rims replacing omphacite. Pargasite shows Al_2O_3 content from 13.96 to 16.67 wt% and Na_2O of 3.48–4.17 wt%. Extremely Al-rich amphibole (sadanagaite) with Al_2O_3 reaching up to 21 wt% replaces garnet.

Sample WOL 1: Quartz-rich eclogite, Wolfsberger Hütte
Sample WOL 1 is a coarse-grained eclogite and consists of garnet, clinopyroxene, clinozoisite, amphibole, quartz, rutile, titanite, and minor ilmenite (Figure 2b). Zircon and apatite are accessory phases. Garnet crystals are anhedral and occur as two types: (1) smaller garnet crystals (<1.5 mm) that show relatively weak, patchy compositional zoning, and (2) larger garnet crystals (<3.5 mm) with more distinct zoning (Figure 7). Altogether, garnet is almandine-rich and frequently contains inclusions of omphacite, quartz, rutile, titanite, clinozoisite, and apatite. High-precision X-ray maps indicate typical prograde zoning with high X_{Mn} and $\text{Fe}/(\text{Fe}+\text{Mg})$ in the core and X_{Mg} increasing from core to rim. The overall composition of garnet is

$\text{Am}_{45-52}\text{Grs}_{26-34}\text{Prp}_{14-26}\text{Sps}_{0.2-2.0}$. The Lu distribution in the smaller garnets shows a small central peak and enrichment in the rim domains, whereas the larger crystals display Lu peaks only close to the rims (Figure 7). Omphacite is the second most abundant mineral phase after garnet. It is unzoned and occurs as large anhedral grains in the matrix as well as small inclusions in garnet. It contains 23% to 39% jadeite component in addition to 1–4% acmite component. Occasionally, omphacite is replaced by Na-poor clinopyroxene (Jd_{15}) + sodic plagioclase (An_{6-16}) + calcic amphibole. Amphibole is present as poikiloblasts in the matrix or as part of symplectitic aggregates replacing omphacite. This amphibole is pargasite with Al_2O_3 content between 12.97 and 16.22 wt% and less variable Na_2O between 2.97 and 3.88 wt%. Kelpitic amphibole containing up to 20 wt% Al_2O_3 occurs at the contact with garnet. Clinozoisite appears in textural equilibrium with omphacite and garnet. Matrix clinozoisite and inclusions in garnet display similar compositions with low Fe_2O_3 ranging between 1.25 and 2.52 wt%. Rutile is present as inclusions in garnet, but also commonly as subhedral grains in the matrix, locally rimmed by titanite. The latter is frequent also as inclusion in garnet

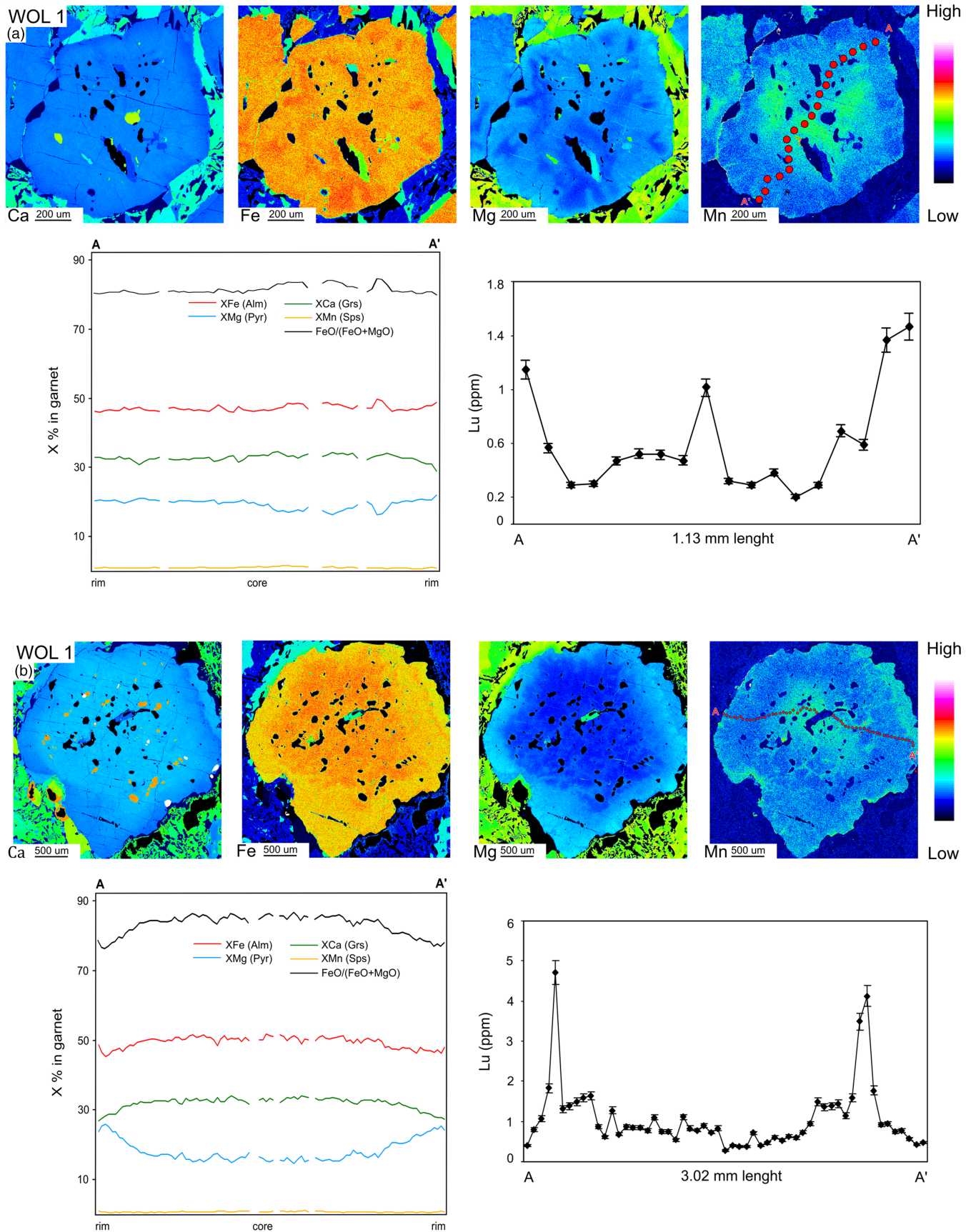


FIGURE 7 Major element distribution maps of representative garnet crystals from sample WOL 1. (a) Small garnet with patchy major element compositional zoning shows a bell-shaped distribution of Lu indicating prograde garnet growth. (b) Larger garnet crystals show prograde major element zoning, whereas Lu is concentrated near the rims. See text for details [Color figure can be viewed at wileyonlinelibrary.com]

porphyroblasts. Ilmenite is the least abundant Ti-phase and occurs only in association with rutile. Observations suggest that ilmenite grew first, followed by rutile then titanite, in line with a clockwise pressure-temperature evolution (e.g., Zack & Kooijman, 2017).

4.1.3 | Sieggraben

Sample SIG 3

The eclogite from Sieggraben is coarse-grained and contains garnet, clinopyroxene, amphibole, epidote, rutile, titanite, plagioclase, and quartz (Figure 2g). Garnet crystals are anhedral to subhedral and reach up to 2.5 mm in size. Garnet is almandine-rich and encloses amphibole, plagioclase, epidote, K-feldspar, quartz, rutile, titanite, and ilmenite. Composition of garnet is $\text{Am}_{49-55}\text{Grs}_{26-34}\text{Prp}_{11-21}\text{Sp}_{0.3-5.0}$. The grains are zoned and show increasing pyrope and almandine components from core to rim and correspondingly decreasing grossular and spessartine components. The Lu distribution in garnet as well as that of the other heavy REEs shows high concentrations near rims but no discernible central

peaks (Figure 8). Small omphacite crystals with jadeite component of $\sim 24\%$ occur in the matrix (Figure 2g). Most of the omphacite was replaced by symplectites of diopside-rich clinopyroxene (Jd_{9-16}) and albite-rich plagioclase (An_{10-20}) during a retrograde overprint. Calcic amphibole occurs as poikiloblasts, but also as part of narrow symplectite rims replacing omphacite. Amphibole displays Al_2O_3 content varying between 10.44 and 17.97 wt% and Na_2O content ranging from 2.31 to 3.16 wt%. Kelpithic amphibole (sadanagaite) replacing garnet shows Al_2O_3 of at least 19 wt%. Clinzoisite occurs as single grains in textural equilibrium with garnet and amphibole (Figure 2g). The Fe_2O_3 content is somewhat higher than in the previous samples and ranges from 7.64 to 8.46 wt%. Inclusions in garnet are epidote-rich and contain up to 15.31 wt% Fe_2O_3 . Plagioclase occurs as inclusions in garnet as well as symplectites with clinopyroxene and amphibole after breakdown of omphacite. Rutile and ilmenite are abundant in the matrix and occur as irregular grains. Rutile inclusions in garnet are present as single grains or partly replaced by titanite. Titanite is mainly present as single inclusions in garnet.

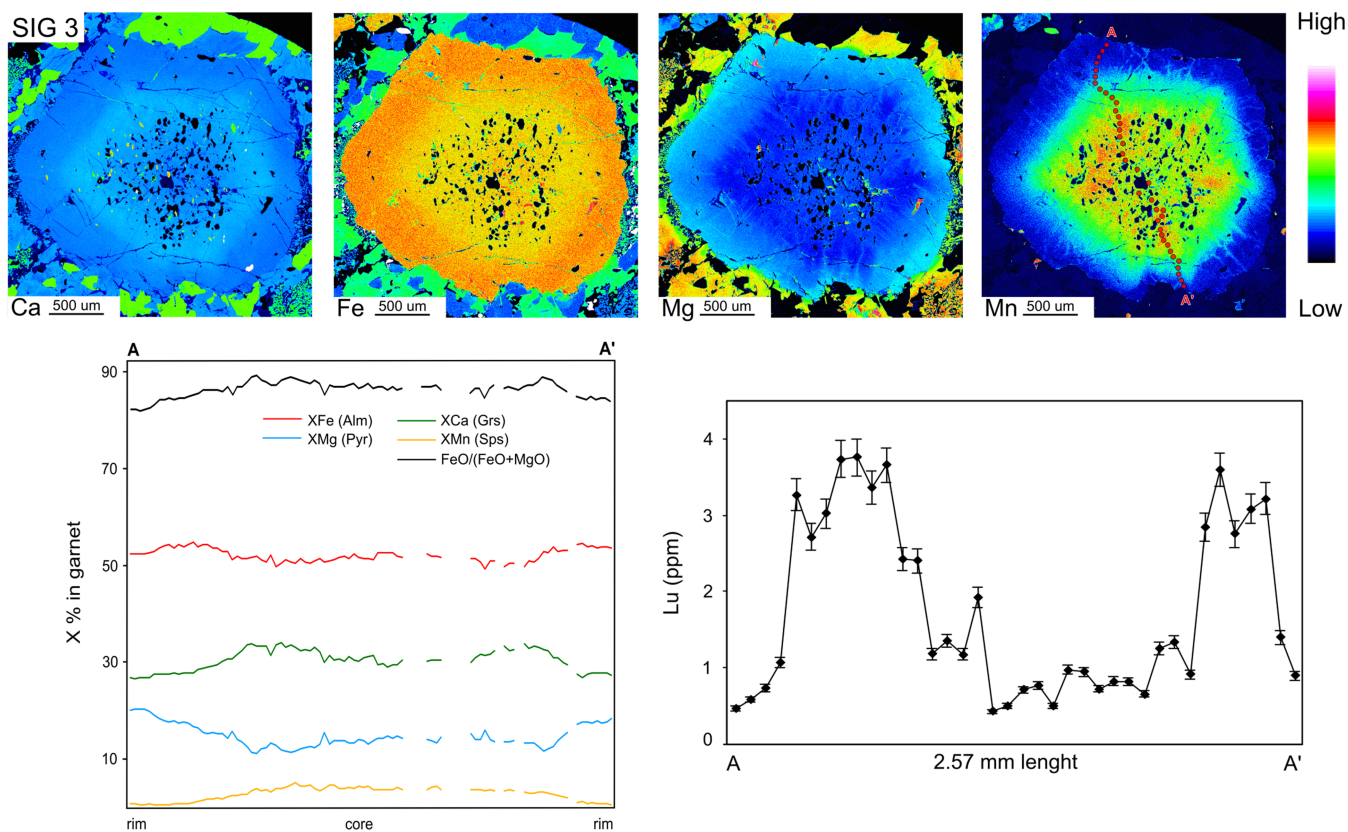


FIGURE 8 Major element distribution maps of a representative garnet from sample SIG 3. Compositional profiles show bell-shaped distribution indicating prograde garnet growth. The distribution of Lu shows elevated concentrations near the garnet rims, whereas a central peak is missing. See text for details [Color figure can be viewed at wileyonlinelibrary.com]

4.1.4 | Texel complex

Sample SAL 1, Saltaus valley

Sample SAL 1 is fine- to medium-grained eclogite composed of garnet, omphacite, amphibole, rutile, ilmenite, quartz, and minor titanite and epidote. Fine-grained symplectites locally replace omphacite in the matrix (Figure 2h). They are made up of diopside-rich clinopyroxene, plagioclase, and calcic amphibole. Accessory zircon can be found as single grains in the matrix and as inclusions in garnet. The sample displays a weak foliation defined by elongated omphacite and aligned amphibole.

The garnets are subhedral to anhedral and reach up to 1 mm in size. They are almandine-rich and clearly show two growth stages (Figure 9). Idiomorphic Grt 1 displays compositional zoning with high spessartine and grossular components in the core and increasing pyrope component toward the rims. The overall composition of Grt 1 is $\text{Alm}_{53-65}\text{Grs}_{15-35}\text{Prp}_{8-20}\text{Sps}_{0.5-2.4}$. An abrupt change in chemical composition marks the second garnet growth stage (Grt 2). It is characterized by a sharp

increase in Ca-content, as well as a decrease in Mg- and Fe-contents relative to the rims of Grt 1 (Table 4). Inclusions of omphacite, quartz, amphibole, rutile, titanite, epidote, plagioclase, zircon, and apatite are abundant in Grt 1 and along the boundary between Grt 1 and Grt 2. Grt 2 is inclusion-free. The distribution of Lu mimics well the zoning of the Ca and Mn in garnet (Figure 9). The core of Grt 1 is characterized by the highest Lu concentrations, which decrease toward Grt 2, where it is increasing again. Omphacite occurs as large, anhedral crystals in the matrix with 37–48% Jd component. They are unzoned and contain inclusions of quartz and amphibole. Smaller aggregates among the symplectitic matrix have lower jadeite component that ranges between 25% and 34% (Figure 2h; Table 4). Larger and smaller omphacite crystals with the same compositions are also included in garnet. Locally, symplectites of diopside-rich clinopyroxene and albite-rich plagioclase (An_{2-8} and rarely An_{13-18}) replace omphacite in the matrix. The symplectitic pyroxene contains 19–21% jadeite. Amphibole with katophorite composition (Hawthorne

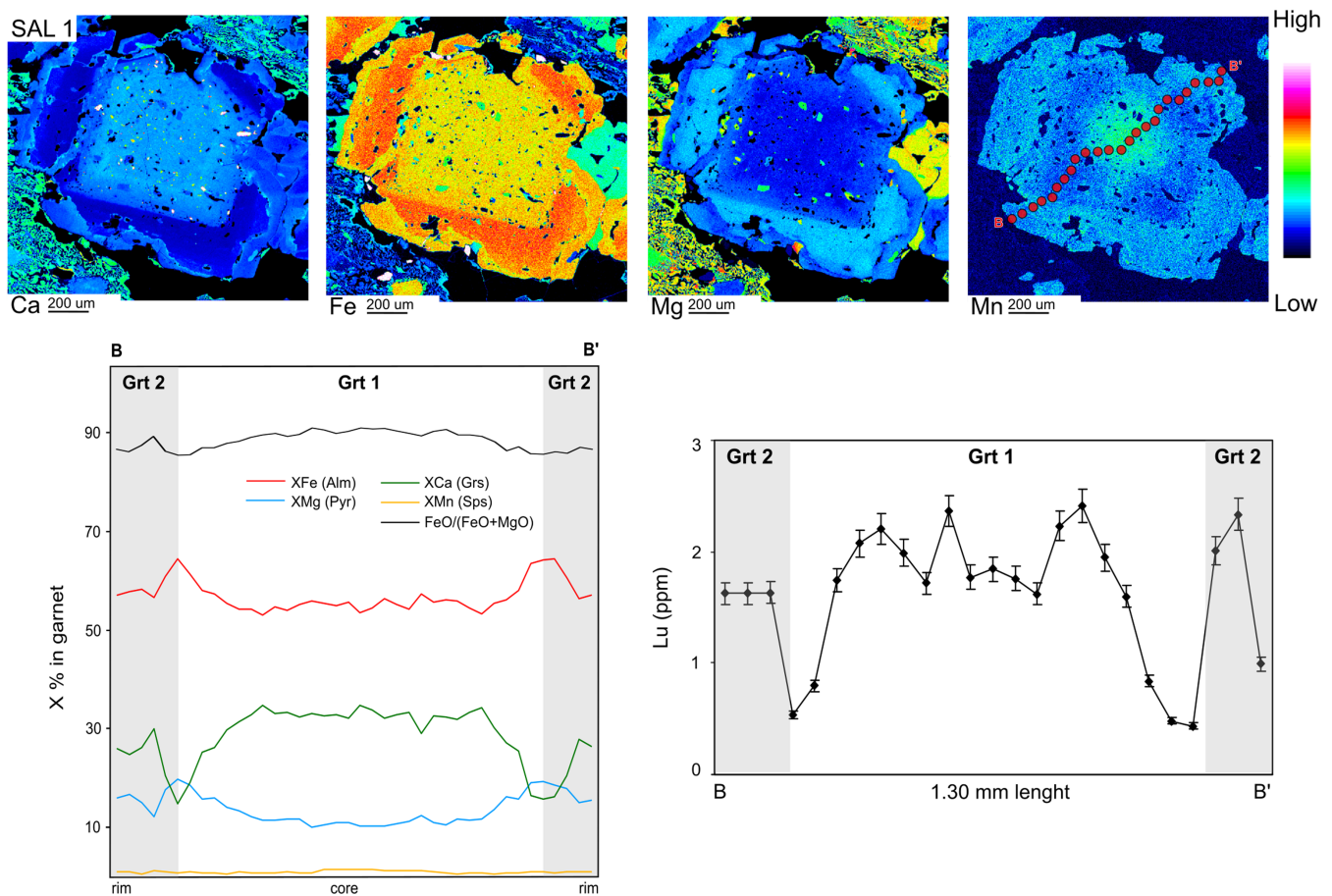


FIGURE 9 Major element distribution maps of a representative garnet from sample SAL 1. Compositional and Lu concentration profiles follow the trace B-B' indicated on the map. They clearly show the presence of two growth phases (Grt 1 and Grt 2). The bell-shaped pattern of Lu indicates preserved prograde growth zonation [Color figure can be viewed at wileyonlinelibrary.com]

et al., 2012) occurs in textural equilibrium with omphacite and garnet in the matrix, indicating crystallization during high-pressure conditions. Its Al_2O_3 content ranges between 10.35 and 13.32 wt% and Na_2O reaches up to 4.74 wt% (Table 4). The retrogressive amphiboles have pargasitic composition. They form symplectites together with plagioclase and clinopyroxene or replace coarse-grained primary amphiboles. Extremely Al-rich amphiboles (up to 20 wt% Al_2O_3) replacing garnet are reaction products from garnet during decompression. Most of the amphibole inclusions in garnet are pargasite and rarely katophorite with compositions similar to the matrix amphiboles, suggesting that pargasite inclusions actually reflect reequilibrated inclusions. Rutile is abundant as inclusions in garnet. In the matrix rutile occurs as single grains or replaces ilmenite. Sometimes both phases are rimmed by titanite. Inclusions of pure titanite are observed mainly in the garnet core, while matrix titanite is always associated with ilmenite and rutile.

4.2 | P-T estimates

In order to better constrain the metamorphic evolution of the eclogites from the Austroalpine high-pressure belt, equilibrium phase diagram modelling was used to estimate the peak metamorphic conditions of the studied samples. Equilibrium phase diagrams are calculated from XRF-determined whole rock compositions and compared with observed assemblages as well as mineral compositions of garnet, omphacite, amphibole, and plagioclase obtained by electron microprobe analyses (Tables 3 and 4). We used the software package Theriak/Domino (de Capitani & Petrakakis, 2010) together with a modified thermodynamic dataset of Holland and Powell (1998). Non-ideal solution models for garnet (White et al., 2007), clinopyroxene (Green et al., 2007), and amphibole (Diener et al., 2007) were used for the calculations. The system was assumed to be saturated in pure water. The Si-Al-Fe-Mg-Ca-Na-O input compositions were calculated assuming bivalent iron and normalized to 100 cations. In order to account for the observed minor trivalent iron in clinozoisite/epidote, omphacite, and amphibole, a small amount of oxygen (up to 1.0 mol) was added. The results are illustrated on Figures 10 and S1 to S6.

4.2.1 | Sample HO 1: Quartz-rich eclogite, Hohl, Koralpe

The inferred stable equilibrium assemblage in sample HO 1 is garnet-omphacite-amphibole-clinozoisite-quartz-rutile. It is predicted to be stable over a relatively large

pressure-temperature range between 1.45 and 2.25 GPa and 580–770°C (Figure 10). However, the observed mineral chemistry corresponds to the upper part of this stability field. This is illustrated via calculated isopleths for grossular and almandine content in garnet, which constrain the peak conditions to ~ 2.2 GPa and 670°C. The intersection between modelled garnet volume isopleths and the corresponding grossular and almandine contents confirm the estimated conditions. This interpretation is in close agreement with the published eclogite peak conditions from this region (1.65–2.05 GPa/620–720°C, Bruand et al., 2010; 2.2–2.8 GPa/635–720°C, Miller et al., 2007, and references therein).

4.2.2 | Sample HO 2: Kyanite-rich eclogite, Hohl, Koralpe

The observed mineral assemblage of sample HO 2 contains garnet-omphacite-kyanite-amphibole-clinozoisite-quartz-rutile, corresponding to 1.8–2.3 GPa and 700–800°C in the phase diagram (Figure 10). These constraints are in line with the published P-T data, which are in the range of 2.2–2.4 GPa and 630–785°C (Miller et al., 2007; Miller, Thöni, et al., 2005). For more precise estimation of P and T, grossular and pyrope isopleths were calculated. They intersect at ~ 2.2 GPa and 730°C, within the range of the already published data.

4.2.3 | Sample GRÜ 2: Quartz-rich eclogite, Grünburger Bach, Saualpe

The peak mineral assemblage of the quartz-rich eclogite from Grünburger Bach is garnet-omphacite-clinozoisite-quartz-rutile. The predicted stability field for this assemblage extends over a wide pressure-temperature range of 1.7–2.8 GPa and 680–850°C (Figure 10). The observed grossular and almandine contents in garnet correspond to ~ 2.4 GPa and 700°C in the peak assemblage stability field. This result is well in agreement with the published peak conditions of 2.2–2.4 GPa and 629–727°C (Miller et al., 2007; Miller, Thöni, et al., 2005). In addition, garnet volume isopleths reveal that garnet grew under increasing pressure and temperature, similar to sample HO 1.

4.2.4 | Sample WOL 1: Quartz-rich eclogite, Wolfsberger Hütte, Saualpe

Sample WOL 1 contains the high-pressure assemblage garnet-omphacite-clinozoisite-quartz-rutile, which is

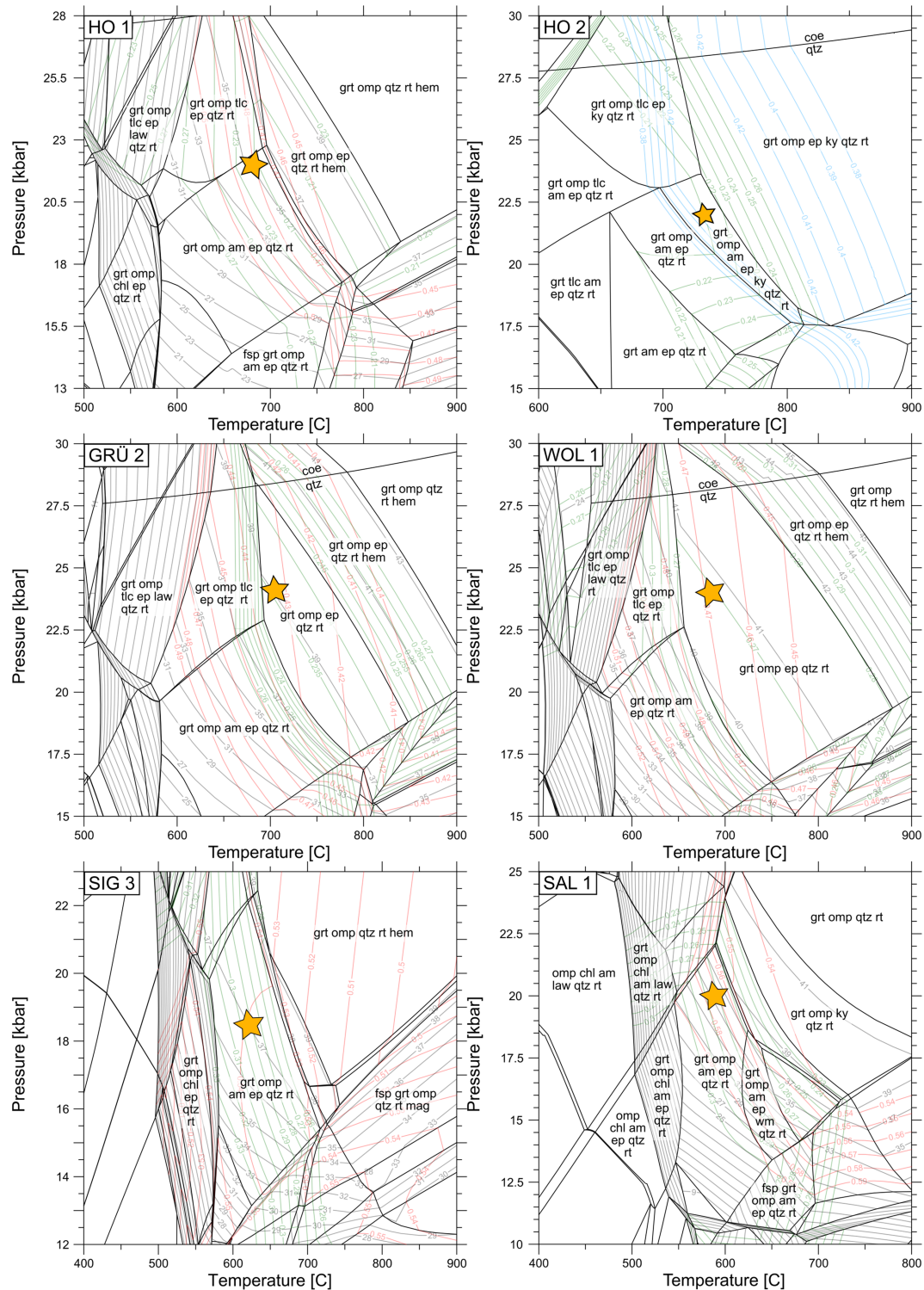


FIGURE 10 Equilibrium phase diagrams calculated for SiAlFeMgCaNaOH bulk compositions of the dated eclogite samples HO 1, HO 2, GRÜ 2, WOL 1, SIG 3, and SAL 1. All calculations assume water saturation. Additionally, compositional isopleths for almandine (red lines), grossular (green lines), and pyrope (blue lines; only for sample HO 2) components in garnet were calculated. Grey isopleths show volume percentage of garnet. The yellow stars correspond to the estimated peak conditions [Color figure can be viewed at wileyonlinelibrary.com]

stable between 1.6–2.8 GPa and 650–870°C in the calculated phase diagram. Equilibrium conditions can be constrained to ~2.4 GPa and 680°C from the compositional

isopleths of garnet. These P-T conditions overlap with those of the quartz-rich eclogites from Grünburger Bach as well as the published data for Saulpe (Miller

et al., 2007; Miller, Thöni, et al., 2005). Similar to the samples described above, modelling of the garnet volume percentage shows that garnet grew along a prograde path under increasing temperature and pressure.

4.2.5 | Sample SIG 3, Sieggraben

The peak pressure assemblage of the Sieggraben eclogite is garnet-omphacite-amphibole-epidote-rutile-quartz. Phase equilibrium modelling predicts a relatively large stability field for this assemblage. The grossular and almandine components that reflect garnet rim composition correspond to peak pressure conditions ranging between 1.7 and 1.9 GPa at 600–650°C. The temperature estimates are in good agreement with the published P-T data for the eclogites from Sieggraben (Kromel et al., 2011; Neubauer, Dallmeyer, et al., 1999), but the estimated peak pressure is higher than previously suggested by these authors (max. 1.7 GPa).

4.2.6 | Sample SAL 1, Saltaus valley, Texel complex

As explained above, the garnets in sample SAL 1 display a two-stage growth history. The obtained Lu-Hf-garnet age (see Section 4.3 below) suggests that the two garnet generations did not grow during a single high-pressure event. In this case, Grt 1, which is also the main garnet generation, is a pre-Alpine relic that was overgrown by Grt 2 during the regional eclogite-facies event in Cretaceous times. The well-developed Grt 2 suggests that matrix minerals are also Eoalpine in age and in equilibrium with Grt 2. It is not possible to reconstruct the P-T conditions of the pre-Alpine metamorphic event.

The Eoalpine peak pressure assemblage is characterized by garnet, omphacite, amphibole, epidote, quartz, and rutile. As a result of the at least two stages of evolution of this eclogite, disequilibrium (e.g., chemical) effects on the effective bulk compositions may be large, and we consider the obtained conditions as a first approximation. The compositional isopleths as well as the amount of garnet indicate that the assemblage is stable within the upper part of the relatively large stability field, i.e., 1.9–2.1 GPa and 570–600°C. This temperature range fits well with the published data for eclogites from Saltaus valley. However, our peak pressures differ strongly from those published in Habler et al. (2006). These authors applied albite-jadeite-quartz barometry and obtained notably lower pressure conditions probably due to its limited application based upon the breakdown of albite (e.g., Page et al., 2003; Tropper et al., 1999). Zanchetta

et al. (2013) proposed UHP metamorphic conditions for the formation of eclogite in Ulfas valley, north of our sample locality, but evidence for that is lacking in samples from Saltaus valley.

4.3 | Geochronology

New Lu-Hf isotope data are presented here for seven eclogite samples from the Austroalpine basement of the Eastern Alps. The results are given in Table 5 and illustrated on Figure 11.

4.3.1 | Sample HO 1 (quartz-rich eclogite) and sample HO 2 (kyanite-rich eclogite) from Hohl, Koralpe

Three garnet separates of each sample as well as selectively digested whole rocks were used to calculate the Lu-Hf isochrons. Additionally, an omphacite fraction from sample HO 1 was handpicked and analysed. The garnet fractions of both samples show distinctly different $^{176}\text{Lu}/^{177}\text{Hf}$ of 2.65–2.74 for HO 1 and 0.81–1.09 for HO 2. The Hf concentration in the garnets of HO 1 range from 86 to 93 ppb, and in the garnets of HO 2 from 73 to 79 ppb. The Lu-Hf ages are 98.80 ± 0.65 Ma (MSWD 1.3; $n = 5$) for HO 1 and 92.6 ± 2.0 Ma (MSWD 0.35; $n = 4$) for HO 2.

4.3.2 | Samples GRÜ 1 and GRÜ 2 (quartz-rich eclogite) from Grünburger Bach, Saualpe

Garnet and omphacite separates as well as table top digested whole rock aliquots were used for the calculations of the isochrons for samples GRÜ 1 and GRÜ 2. Both samples show very similar isotopic compositions with Hf concentration in the garnets ranging from 119 to 134 ppb and $^{176}\text{Lu}/^{177}\text{Hf}$ ratio between 1.19 and 1.34. Omphacites contain Hf concentrations of 595 and 623 ppb and $^{176}\text{Lu}/^{177}\text{Hf}$ of 0.00429 and 0.00329, respectively. The resulting ages are 100.3 ± 1.0 Ma (MSWD 1.03; $n = 5$) for GRÜ 1 and 101.79 ± 0.92 (MSWD 1.01; $n = 5$) for GRÜ 2, both identical within error.

4.3.3 | Sample WOL 1 (quartz-rich eclogite) from Wolfsberger Hütte, Saualpe

Three handpicked garnet separates and one table top digested whole rock sample were used to determine the age of sample WOL 1. The $^{176}\text{Lu}/^{177}\text{Hf}$ ratio of the

TABLE 5 Lu-Hf isotope compositions of eclogites from the Eastern Alps

Samples	ppm Lu	ppm Hf	$^{176}\text{Lu}/^{177}\text{Hf}$	2 s.d.	$^{176}\text{Hf}/^{177}\text{Hf}$	2 s.d.	Age (Ma)
GRÜ 1							
WR tt	0.544	0.596	0.1296	0.0003	0.283321	0.000018	100.3 ± 1.0
WR b	0.544	2.00	0.03871	0.00008	0.283165	0.000020	99.8 ± 1.2
Omp	0.0180	0.595	0.004292	0.000009	0.283093	0.000024	
Grt 1	1.16	0.133	1.232	0.002	0.285402	0.000024	
Grt 2	1.14	0.134	1.203	0.002	0.285312	0.000034	
Grt 3	1.18	0.129	1.294	0.003	0.285508	0.000035	
GRÜ 2							
WR tt	0.482	0.600	0.1141	0.0002	0.283300	0.000017	101.79 ± 0.92
WR b	0.498	2.18	0.03244	0.00006	0.283127	0.000030	102.2 ± 1.5
Omp	0.0170	0.623	0.003886	0.000008	0.283072	0.000024	
Grt 1	1.12	0.134	1.185	0.002	0.285326	0.000018	
Grt 2	1.12	0.119	1.340	0.003	0.285626	0.000027	
Grt 3	1.11	0.130	1.211	0.002	0.285416	0.000062	
HO 1							
WR tt	0.536	0.605	0.1256	0.0003	0.283248	0.000015	98.80 ± 0.65
WR b	0.544	2.22	0.03480	0.00007	0.283118	0.000021	97.97 ± 0.71
Omp	0.0238	0.625	0.005419	0.000011	0.283003	0.000037	
Grt 1	1.72	0.0925	2.647	0.005	0.287921	0.000048	
Grt 2	1.66	0.0861	2.735	0.005	0.288030	0.000048	
Grt 3	1.72	0.0888	2.744	0.005	0.288093	0.000054	
HO 2							
WR 1 tt	0.119	0.248	0.06813	0.00014	0.283329	0.000039	92.6 ± 2.0
WR 2 tt	0.118	0.248	0.06778	0.00014	0.283330	0.000024	
Grt 1	0.561	0.0734	1.086	0.002	0.285096	0.000035	
Grt 2	0.501	0.0779	0.9137	0.0018	0.284742	0.000195	
Grt 3	0.448	0.0787	0.8089	0.0016	0.284578	0.000081	
SAL 1							
WR 1 tt	0.944	0.471	0.2848	0.0006	0.284134	0.000034	232.0 ± 6.4
WR 2 tt	0.959	0.424	0.3207	0.0006	0.284256	0.000029	
WR b	0.983	4.87	0.02863	0.00006	0.283081	0.000022	231 ± 10
Grt 1	2.56	0.0567	6.448	0.013	0.310865	0.000062	
Grt 2	2.54	0.0554	6.539	0.013	0.311817	0.000078	
Grt 3	2.53	0.0495	7.286	0.015	0.314069	0.000067	
SIG 3							
WR 1 tt	0.434	0.656	0.09375	0.00019	0.283330	0.000019	89.89 ± 0.37
WR 2 tt	0.424	0.670	0.08972	0.00018	0.283325	0.000025	
WR 3 tt	0.428	0.662	0.09177	0.00018	0.283317	0.000022	
WR b	0.438	1.69	0.03676	0.00007	0.283208	0.000026	90.12 ± 0.43
Grt 1	3.11	0.0830	5.319	0.011	0.292100	0.000056	
Grt 2	3.16	0.0861	5.216	0.010	0.291933	0.000064	
Grt 3	3.17	0.0776	5.805	0.012	0.292921	0.000060	

(Continues)

TABLE 5 (Continued)

Samples	ppm Lu	ppm Hf	$^{176}\text{Lu}/^{177}\text{Hf}$	2 s.d.	$^{176}\text{Hf}/^{177}\text{Hf}$	2 s.d.	Age (Ma)
WOL 1							
WR tt	0.584	0.650	0.1277	0.0003	0.283279	0.000017	101.0 ± 1.2
WR b	0.590	2.30	0.03643	0.00007	0.283079	0.000020	101.9 ± 1.2
Grt 1	1.47	0.119	1.754	0.004	0.286370	0.000059	
Grt 2	1.51	0.125	1.717	0.003	0.286246	0.000062	
Grt 3	1.49	0.119	1.782	0.004	0.286407	0.000051	

garnets ranges from 1.72 to 1.78, and their Hf concentration is between 119 and 125 ppb. The age is 101.0 ± 1.2 Ma (MSWD 0.87; $n = 4$). An isochron calculated with the completely digested whole rock sample yields an identical age. The age is also identical with both ages from Grünburger Bach.

4.3.4 | Sample SIG 3 from Siegraben

Three garnet separates and one selectively digested whole rock aliquot from sample SIG 3 were used to determine its age. The garnets display Hf concentrations between 78 and 86 ppb and $^{176}\text{Lu}/^{177}\text{Hf}$ of 5.22–5.81. The age is 89.89 ± 0.37 Ma (MSWD 0.15; $n = 4$). A second isochron, calculated using the completely digested whole rock gives the same age within the error limits.

4.3.5 | Sample SAL 1 from Saltaus valley, Texel complex

For sample SAL 1, three garnet separates and whole rock aliquot define a statistically insignificant isochron with mean square weighted deviates (MSWD) >74 (Figure 11). The resulting Lu-Hf age of 232.0 ± 6.4 Ma ($n = 5$) indicates a variable mixing of Alpine (Grt 2) and relic pre-Alpine garnets (Grt 1).

5 | DISCUSSION

5.1 | Interpretation of the Lu-Hf ages: Prograde garnet growth versus cooling

A crucial factor for the interpretation of Lu-Hf ages is identification of the growth mechanisms of garnet as well as the major and trace element zoning. Particularly, REE patterns can provide valuable information about the processes that operated during garnet growth (e.g., Hickmott et al., 1987). Two rate-limiting end-member processes for

porphyroblast growth have been discussed in numerous studies, i.e., interface- and diffusion-controlled growth (e.g., Carlson, 1989; Daniel & Spear, 1999; Fischer, 1978; Hyppolito et al., 2018; Kretz, 1974; Skora et al., 2005; Skora et al., 2006; Spear & Daniel, 1998, 2001). Interface-controlled garnet growth implies that the attachment or incorporation of material at the garnet surface is relatively slow compared to diffusion to the growing garnet. Thus, pre-existing garnet crystals do not influence the nucleation of new ones. Moreover, garnet will be randomly distributed in a homogeneous matrix and will grow with equal radial increments regardless of size. When the diffusion of material to the growing garnet is slower compared to the growth rate, then growth is diffusion-controlled. This may result in the development of a depletion rim around growing porphyroblasts, which suppresses nucleation adjacent to the growing garnet. Therefore, garnet crystals will have a non-random distribution in a homogenous matrix, where smaller garnet appears at greater distances to large garnet.

Regarding the Lu-Hf system, a key assumption is that garnet remains an isotopically closed system since crystallization. Hence, Lu and Hf are effectively retained in the garnet and do not undergo substantial diffusional reequilibration that modifies primary Lu-Hf isotope systematics during the thermal peak of metamorphism and/or consequent cooling of the system. However, rates and mechanisms of element diffusivity in garnet depends on several other factors in addition to temperature: e.g., grain size, oxygen fugacity, cooling rate, ionic charge, presence or absence of fluid (e.g., Bloch et al., 2015; Caddick et al., 2010; Skora et al., 2006; Smit et al., 2011). Experimental studies showed that the ionic charge of an element is a major control factor on its diffusive closure temperature, i.e., 2+ ions (e.g., Mn^{2+}) diffuse by orders of magnitude faster than 3+ (e.g., Lu^{3+}), whereas the diffusion of 4+ (e.g., Hf^{4+}) is even slower (e.g., Bloch et al., 2015; Carlson, 2006, 2012; Ganguly et al., 1998; van Orman et al., 2002). The published estimates of the closure temperature of the Lu-Hf system

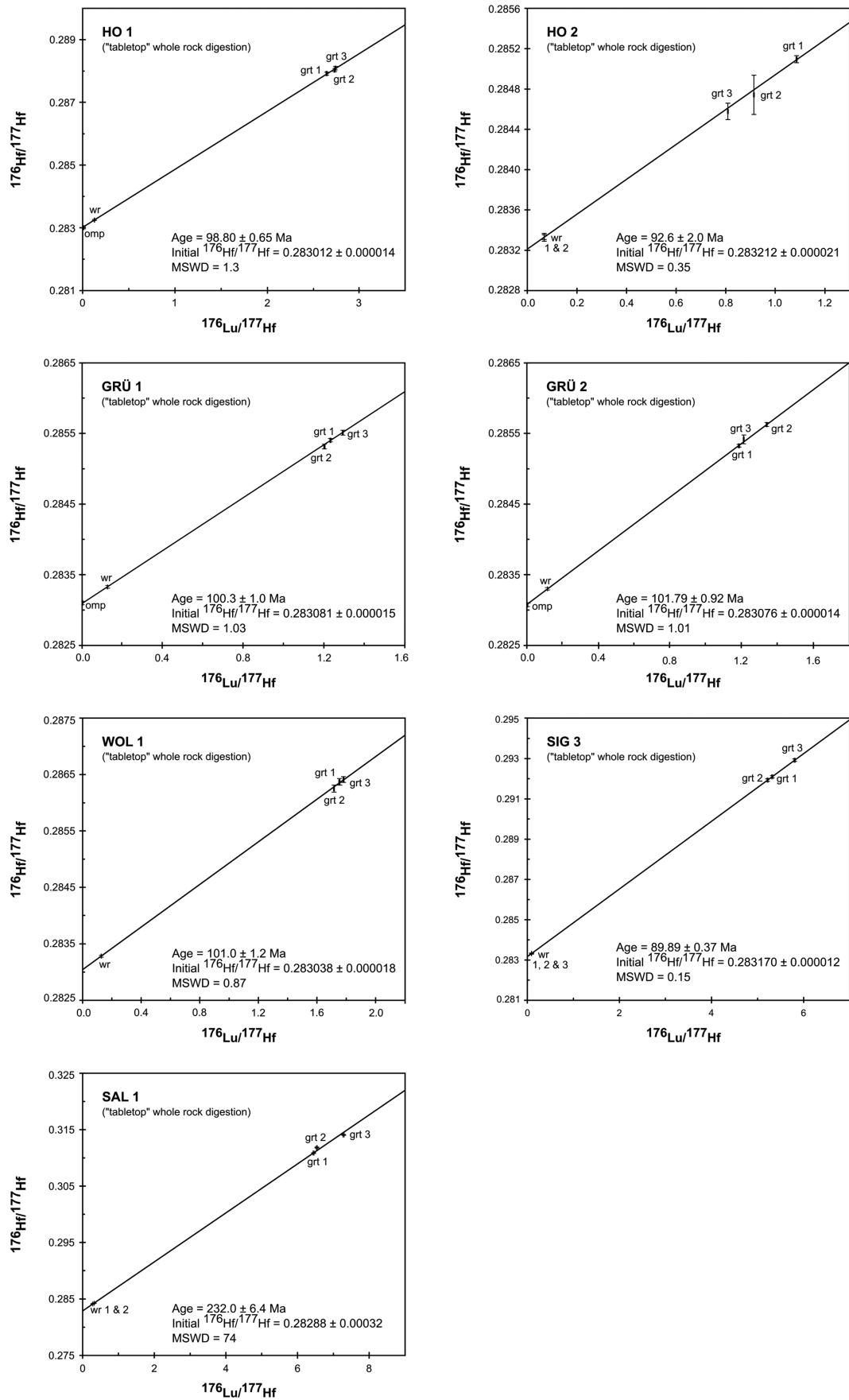


FIGURE 11 Lu-Hf isochron plots for the dated eclogite samples. Grt, garnet digestion; omp, omphacite digestion; wr, whole rock. The error bars are typically smaller than the symbol

appear to be in the range of $\sim 800\text{--}850^\circ\text{C}$ for garnets with 1 mm diameter (Smit et al., 2013; van Orman et al., 2002), thus well above the peak temperature estimates for the eclogites from the Austroalpine high-pressure belt, which experienced a thermal peak at $\leq 730^\circ\text{C}$.

As described above, garnet grains from samples HO 1, GRÜ 1, and GRÜ 2 exhibit compositional zoning with high Ca and Mn distributions as well as bell-shaped Lu concentration patterns in the cores (Figures 3, 5, and 6). This means that the garnets have preserved their prograde growth zonation pattern for Lu-Hf. Therefore, the obtained Lu-Hf ages of 98.80 ± 0.65 Ma, 100.3 ± 1.0 Ma, and 101.79 ± 0.92 (Figure 11), respectively, clearly reflect the time of garnet growth during increasing P and T.

The garnets in the kyanite-rich eclogite HO 2 show a complete homogenization in the distribution of major elements. Unfortunately, due to the very abundant inclusions in the garnet cores as well as the very low concentrations of REE, it was not possible to obtain Lu concentration profiles within the framework of this study. Samples HO 1 and HO 2 belong to the same eclogite body, but the obtained Lu-Hf age of 92.6 ± 2.0 Ma from HO 2 is c. 6 Ma younger than the prograde age of HO 1 (Figure 11). This age discrepancy could be attributed to prolonged (>6 Ma-long) garnet growth in these eclogites. However, further analyses of more garnets would be necessary to resolve this. On the other hand, P-T equilibrium modelling for sample HO 2 constrains somewhat higher temperature ($\sim 730^\circ\text{C}$; Figure 10) than for HO 1 ($\sim 670^\circ\text{C}$), which could suggest that the kyanite-rich eclogite recorded the thermal peak of metamorphism. Hence, the younger age dates the onset of cooling after temperature peak.

As described above, the small garnets in sample WOL 1 display somewhat less pronounced major element zoning, but a distinct Lu concentration peak in the garnet cores (Figure 7). By contrast, the major element composition of the large garnets shows typical prograde growth zoning with Ca-, Fe-, and Mn-poor and Mg-rich rims. However, the corresponding Lu profile shows maxima only near the garnet rims, probably resulting from a depletion halo surrounding the garnet grains early in their growth history (e.g., Skora et al., 2006). The measured Lu profiles in the garnets from sample WOL 1 may be explained by a model in which incorporation of Lu is controlled by diffusion, whereas the overall garnet growth is dominated by the interface-controlled mechanism. Nevertheless, the zoning does not necessarily bias the obtained Lu-Hf age of 101.0 ± 1.2 Ma. In fact, considering the prograde major element zoning pattern and the nearly identical ages of the adjacent GRÜ 1 and GRÜ 2 (100.3 ± 1.0 Ma and 101.79 ± 0.92 , respectively), we

interpret the obtained age to represent prograde garnet growth.

The major element distribution in garnet of sample SIG 3 shows distinct zoning with high Mn- and Ca-contents in the garnet core, whereas Mg and Fe are enriched at the rims (Figure 8). In contrast, Lu is concentrated near the rims and shows no central peak. Similar to WOL 1, we suggest that diffusion-controlled garnet growth is responsible for this pattern. Another possibility is that a very narrow central peak of Lu may have been missed if garnet was not sectioned precisely through its centre. If so, the near-rim peaks would represent a secondary maximum of Lu that was released from the decomposition of REE-bearing minerals within the adjacent matrix (e.g., Fassmer et al., 2016; Konrad-Schmolke et al., 2008). In any case, the REE pattern in the garnets of that sample does not seem to have experienced significant partial resetting during crystallization that could affect the Lu-Hf age. Therefore, the age of 89.89 ± 0.37 Ma is interpreted to be related to burial during subduction.

Both growth stages in the garnets from sample SAL 1 (Grt 1 and Grt 2) record prograde growth zoning with high contents of spessartine and grossular in the inner parts (Figure 9). The Lu concentration through garnet also shows a bell-shaped distribution in Grt 1 and a second enrichment towards the rims (Grt 2). Hence, we interpret the estimated P-T conditions to reflect prograde growth of Grt 2 during subduction. However, the obtained 'Triassic' age (232.0 ± 6.4 Ma; Figure 11) seems to be a mixed result between significantly different garnet age components, most probably pre-Alpine (Grt 1) and Alpine (Grt 2) garnet. By using a mass balance approach (e.g., Kellett et al., 2014), we compared the Lu concentration in the garnet core versus garnet rim and estimated the relative contribution of these zones to the bulk Lu-Hf age. Using average core and rim Lu concentrations and average garnet diameters, we estimated that Grt 1 is responsible for roughly 75% of the total Lu budget in the Texel eclogite (see the supporting information for details of the calculations), which suggests that most of the garnet is pre-Alpine and there is a significant 'contamination' on the age by Alpine garnets that grew during the Eoalpine high-pressure event. Unfortunately, a geologically meaningful age cannot be assigned to any of the growth stages. It could be that pre-Alpine Grt 1 is a relic from the Permian-Triassic high-temperature metamorphism that reached peak pressure conditions at circa 280–260 Ma (Schuster & Stüwe, 2008). However, the Texel complex continues around the Eoalpine Schneeberg Complex (e.g., Sölva et al., 2001) into the Ötztal basement, which contains Variscan eclogites. Together with

the recent Lu-Hf garnet dating of eclogites from Schobergruppe, where both Variscan and Alpine ages were obtained (Hauke et al., 2019), this suggests that the pre-Alpine garnets from Texel are Variscan as well.

5.2 | Tectonic implications

A compilation of garnet-whole rock ages from this and other studies is shown in Figure 12a (Hauke et al., 2019; Sandmann et al., 2016; Thöni et al., 2008). The oldest ages of c. 100 Ma are located in the Koralpe and Saualpe,

previously interpreted as relating to burial. This area is also characterized by intense igneous and metamorphic activity of regional importance during the Permian–Triassic period (e.g., Schuster et al., 2001). The gabbroic protoliths of the Koralpe-Saualpe eclogites were derived from a depleted mantle source (Miller et al., 1988, 2007; Miller & Thöni, 1997; Thöni & Jagoutz, 1992) and embedded within the thinned crust of a rift zone that was probably located northwest of the Meliata-Hallstatt Ocean (Figure 11a; Janák et al., 2004; Schuster et al., 2001; Schuster & Stüwe, 2008). This suggests intracontinental subduction initiation, localized by the reactivated Permian rift.

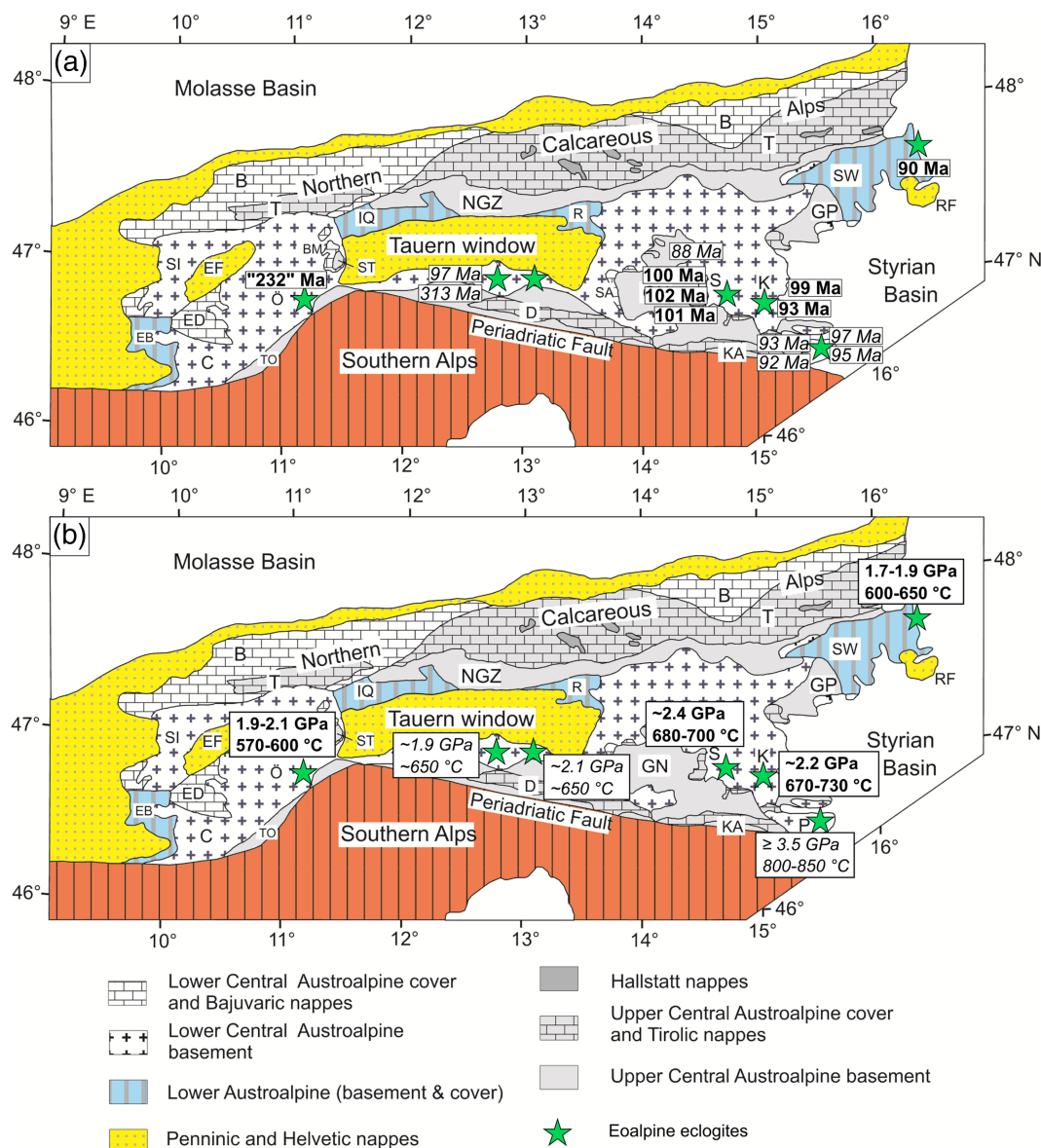


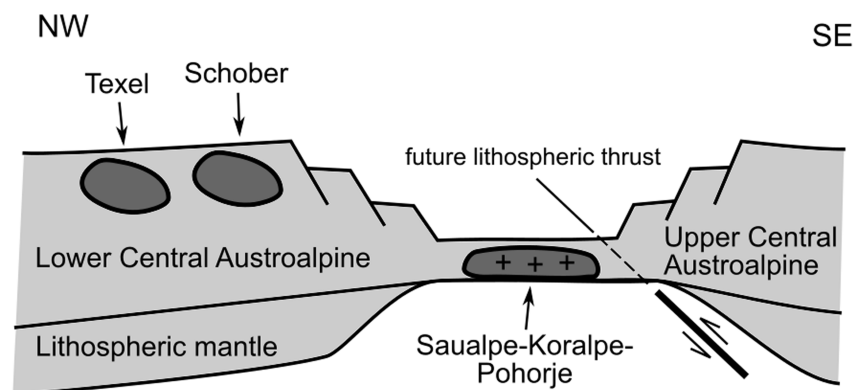
FIGURE 12 (a) Compilation of Lu-Hf garnet ages established in the Austroalpine HP belt (data from Hauke et al., 2019; Sandmann et al., 2016; Thöni et al., 2008; and this study). (b) Compilation of the estimated P-T conditions (data from Hauke et al., 2019; Janák et al., 2015; Konzett et al., 2012; and this study). Bold numbers represent the data obtained in this study [Color figure can be viewed at wileyonlinelibrary.com]

Further south, the eclogites from Pohorje Mountains are also derived from MORB-type gabbroic protoliths, just as the ones in Saualpe and Koralpe (Figure 13a; Miller, Mundil, et al., 2005; Miller et al., 2007; Thöni & Jagoutz, 1992). Protolith ages are not known from the eclogites, but zircon cores in surrounding paragneisses (Janák et al., 2009) and magmatic zircons in orthogneisses (Chang et al., 2020) yielded Permian to Early Triassic ages, suggesting a Permian rift situation also in Pohorje. Lu-Hf dating of these eclogites as well as garnet peridotites yields ages of ~ 95 Ma (Sandmann et al., 2016; Thöni et al., 2008). These ages were interpreted to reflect garnet growth during progressive subduction. This rock complex experienced UHP metamorphism at ≥ 3.5 GPa/800–850°C during the Eoalpine subduction event (Janák et al., 2015), whereas Saualpe-Koralpe reached only 2.2–2.4 GPa/670–700°C. Altogether, this may be explained in two ways. Either, Pohorje and Saualpe-Koralpe are two distinct coherent terranes, and while Pohorje was still being subducted,

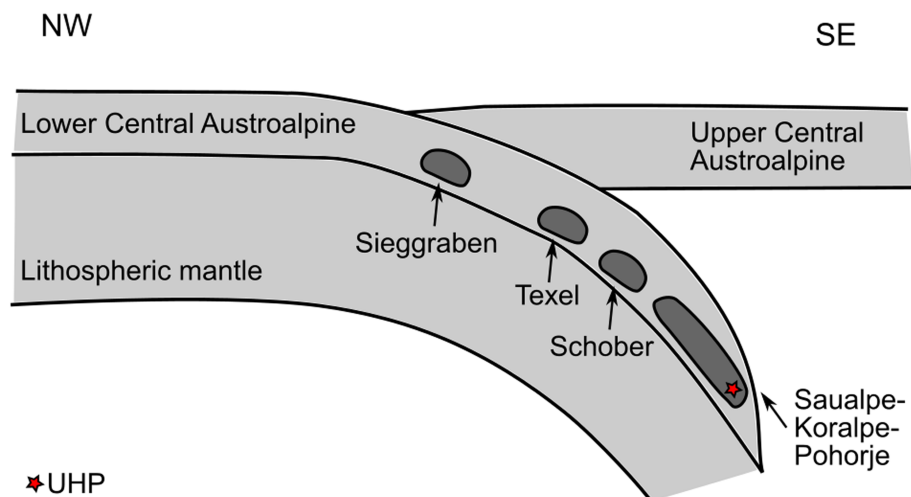
Saualpe-Koralpe had already been accreted to the upper plate. Alternatively, they may represent one single terrane (Figure 13b) and the c. 100 Ma ages from Koralpe and Saualpe reflect an earlier stage of the subduction, while the c. 95 Ma ages from Pohorje reflect a later stage of the P-T path. The occurrence of a ~ 99 Ma quartz-rich eclogite and a ~ 93 Ma kyanite-rich eclogite together in one locality (Hohl) in the southern part of the Koralpe, i.e., rather close to Pohorje, speaks for this second explanation. The two eclogites from Hohl, although they yield different ages, must belong to the same terrane because they were sampled in the same eclogite lens, only a few tens of metres apart.

After Saualpe-Koralpe-Pohorje, subduction continued including the polymetamorphic basement of Schobergruppe and Texel complex (Figure 13b), which comprises rocks with pre-Alpine and Eoalpine overprint. U-Pb zircon and Sm-Nd garnet dating of these complexes yielded only Cretaceous ages (Habler et al., 2006; Linner, 1999; Zanchetta et al., 2013). A recent detailed

(a) Late Permian (c. 255 Ma):



(b) Late Cretaceous (c. 95 Ma):



★ UHP

FIGURE 13 Tectonic model illustrating the proposed evolution of the Austroalpine domain. (a) Gabbroic intrusions embedded within the thinned crust of a rift zone during extension in the Late Permian. (b) Progressive subduction of the Saualpe-Koralpe-Pohorje terrane and the Variscan eclogites from Schobergruppe and Texel complex during the Late Cretaceous [Color figure can be viewed at wileyonlinelibrary.com]

petrological and geochronological study by Hauke et al. (2019) showed that the eclogites from Schobergruppe recorded two high-pressure metamorphic events, Variscan with a minimum age of ~ 314 Ma and Alpine with a maximum age of ~ 97 Ma. They estimated pressure peak conditions during the Late Cretaceous subduction of c. 1.9 GPa and 650°C , whereas the Variscan eclogite experienced conditions of at least 1.6 GPa, as inferred from the amount of garnet.

Similar to the HP rocks from Schobergruppe, previous dating of the eclogites from the Texel complex yielded Late Cretaceous ages. Using Sm-Nd garnet geochronology, Habler et al. (2006) dated eclogites from Saltaus valley as well as their host-rock. The study derived an eclogite age of 85.2 ± 4.6 Ma, which was interpreted to reflect maximum burial stage during subduction. The authors assumed that polyphase garnet growth in the eclogites occurred during a single eclogite-facies metamorphic event. However, the Sm-Nd garnet dating of orthogneisses and metapelites by Habler et al. (2006) resulted in ages of 205.7 ± 5.3 Ma and 208.5 ± 8.4 Ma, respectively, which indicates the presence of pre-Cretaceous mineral relics. Zanchetta et al. (2013) confirmed the Late Cretaceous metamorphic age of the eclogites from Texel by using U-Pb zircon geochronology. They derived an age of 85 ± 4 Ma and considered it to represent a stage near the high-pressure metamorphism. The Lu-Hf garnet dating in this study resulted in a 'Triassic' age of circa 232 Ma. As discussed above, this age is interpreted as a Variscan-Eoalpine mixed age. Considering the distribution of Lu-Hf garnet ages along the Austroalpine high-pressure belt as well as the estimated P-T conditions that show a clear temperature decrease from southeast to northwest (Figure 12a,b), the age of the Alpine metamorphism in the Texel complex should be ≤ 97 Ma.

Accordingly, from c. 97 Ma, continental crust comprising Variscan eclogites was subducted. These rocks were exhumed after the Variscan orogeny and subducted to high-pressure conditions again in the Late Cretaceous. In this scenario, the Texel complex represents the more deeply subducted southeastern part of the Ötztal nappe.

The observed discrepancy between Lu-Hf and Sm-Nd data is common for the eclogites from the Eoalpine high-pressure belt. One reason for that may be the presence of unequilibrated inclusions within garnet that are capable to bias the estimated ages (e.g., Scherer et al., 2000). On the other hand, the different diffusion kinetic properties of Nd^{3+} and Hf^{4+} cause the ^{147}Sm - ^{143}Nd decay system to be more easily affected by diffusive resetting, which leads to a lower closure temperature than that of the ^{176}Lu - ^{176}Hf system in garnet (e.g., Scherer et al., 2000). Thus, the younger Sm-Nd ages can be attributed to the

early stages of cooling from high-grade conditions (e.g., Smit et al., 2013).

All these data suggest that the Eoalpine subduction began at ~ 100 Ma within the Permian rift and lasted until ~ 90 Ma, as inferred from the high-pressure ages from Pohorje and Siegraben. The observed field gradient representing the depth and the timing of the subduction indicate that the Eoalpine high-pressure belt does not represent a subduction-channel mélange, mixing rocks with different P-T history, as suggested by Roda et al. (2012). Rather, it represents one coherent terrane or parts of one terrane that were progressively subducted and accreted in a short phase (~ 10 Ma) of intracontinental subduction. The considerably higher $^{40}\text{Ar}/^{39}\text{Ar}$ hornblende ages from Siegraben, c. 136 to 108 Ma (Neubauer, Dallmeyer, et al., 1999), probably result from excess Ar. Our results show that there is not a continuous record of high-pressure metamorphism in the Austroalpine connecting the Middle (c. 172 Ma) to Late Jurassic (c. 155–152 Ma; Faryad & Henjes-Kunst, 1997) blueschist metamorphism in Meliata with the Cretaceous (c. 100–90 Ma) HP/UHP metamorphism of the Austroalpine. Instead, there is a gap in the record of c. 50 Ma, which speaks against a continuous development from oceanic to continental subduction and rather favours tectonically independent events.

It is well known that P-T conditions of subduction zones depend, among other factors, on subduction rate as well as the relative proportions of oceanic and continental crust being subducted (e.g., Warren, 2013). The higher radiogenic heat production in the continental crust leads to higher temperatures during continental subduction, which only increase with the thickness of the subducted continental crust. Hence, the peak metamorphic temperatures of subducted oceanic crust are usually relatively low ($<600^\circ\text{C}$), whereas those of subducted continental crust may reach up to 800°C . Furthermore, subduction in oceanic subduction zones is usually a long-lasting process, whereas the continental subduction zones are rather short-lived.

The P-T estimations for the Austroalpine eclogites suggest relatively 'warm' conditions on the prograde subduction path (600 – 850°C ; Figure 14), in contrast to the 'cold' Tertiary HP/UHP rocks of the Western Alps (c. 500 – 600°C ; e.g., Dragovic et al., 2020), which originate mainly in an oceanic subduction setting and have much higher P/T ratios, explained by the cooling effect of a subducting oceanic plate (Yamato et al., 2007). This, together with short duration of the Eoalpine subduction cycle (c. 10 Ma), is in line with an intracontinental subduction scenario for the Austroalpine where cooling by a subducting oceanic plate from underneath did not take place.

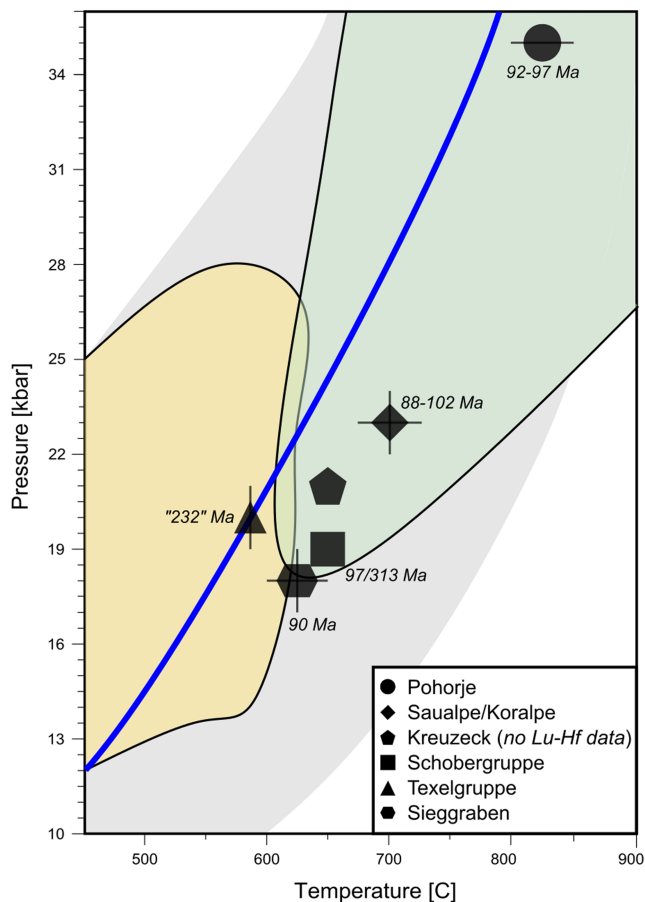


FIGURE 14 Comparison of P-T estimates for the eclogites of the Eoalpine high-pressure belt (age and P-T data from Figure 12). The thick blue line represents the global mean distribution of rock-based P-T estimates for subduction zones with 2σ confidence envelopes (grey area) after Penniston-Dorland, Kohn, and Manning (2015). The yellow field represents P-T data for oceanic subduction rocks that are 175 Ma and younger in age, the green field corresponds to continental subduction environment (after Brown & Johnson, 2019) [Color figure can be viewed at wileyonlinelibrary.com]

6 | CONCLUSIONS

Lu-Hf dating of eclogites from the Austroalpine high-pressure belt yielded prograde garnet growth ages between 101.79 ± 0.92 Ma and 89.89 ± 0.37 Ma, suggesting a short period of (ultra)high-pressure metamorphism. The oldest eclogites are localized in the Saualpe-Koralpe area, where Permian to Triassic gabbros are also widespread. This supports the hypothesis that subduction was intracontinental and was initiated within a pre-existing weakness zone in the lithosphere, a Permian-age rift. The scattered age data from the eclogite from Saltaus valley is explained by the variable mixing between pre-Alpine and Alpine garnets. Therefore, the Texel Complex is interpreted to represent continental crust that contained Variscan high-grade rocks and was

re-subducted during the Eoalpine orogeny. Thermodynamic modelling indicates overall high T/P ratio and gradient with increasing temperatures and pressures from northwest to southeast. There is no continuous record of high-pressure metamorphism linking the Middle to Late Jurassic Meliata blueschist-facies metamorphism with the Cretaceous HP/UHP in the Austroalpine, but instead a gap of 50 Ma, suggesting that these are separate tectonic events.

ACKNOWLEDGEMENTS

We thank Matthijs A. Smit and two anonymous reviewers for their constructive and insightful comments that helped to improve the quality of this manuscript. Editorial handling by C. Warren is highly appreciated. This work was supported by the German Science Foundation (DFG) Grant No. FR700/17-1 to N. Froitzheim and was partly supported by the Slovak Research and Development Agency under grant project APVV-18-0107 to M. Janák.

Open access funding enabled and organized by Projekt DEAL.

DATA AVAILABILITY STATEMENT

The data that support the findings of this study are available from the corresponding author upon reasonable request.

ORCID

Irena Miladinova  <https://orcid.org/0000-0002-2808-0378>

REFERENCES

- Baxter, E. F., & Scherer, E. E. (2013). Garnet geochronology: Time-keeper of tectonometamorphic processes. *Elements*, 9, 433–438.
- Bizzaro, M., Baker, J. A., Haack, H., Ulfbeck, D., & Rosing, M. (2003). Early history of Earth's crust-mantle system inferred from hafnium isotopes in chondrites. *Nature*, 421, 931–933.
- Blichert-Toft, J., Albarède, F., & Kornprobst, J. (1999). Lu-Hf isotope systematics of garnet pyroxenites from Beni Bousera, Morocco: Implications for basalt origin. *Science*, 283, 1303–1306.
- Bloch, E., Ganguly, J., Hervig, R., & Cheng, W. (2015). ^{176}Lu – ^{176}Hf geochronology of garnet I: experimental determination of the diffusion kinetics of Lu^{3+} and Hf^{4+} in garnet, closure temperatures and geochronological implications. *Contributions to Mineralogy and Petrology*, 169, 12.
- Brown, M., & Johnson, T. (2019). Metamorphism and the evolution of subduction on Earth. *American Mineralogist*, 104, 1065–1082.
- Bruand, E., Stüwe, K., & Proyer, A. (2010). Pseudosection modelling for a selected eclogite body from the Koralpe (Hohl), Eastern Alps. *Mineralogy and Petrology*, 99, 75–87.

- Burtman, V., & Molnar, P. (1993). Geological and geophysical evidence for deep subduction of continental crust beneath the Pamir. *Geological Society of America, Special Paper*, 281, 1–70.
- Burton, K. W., Kohn, M. J., Cohen, A. S., & O’Nions, R. K. (1995). The relative diffusion of Pb, Nd, Sr and O in garnet. *Earth and Planetary Science Letters*, 133, 199–211.
- Caddick, M. J., Konopásek, J., & Thompson, A. B. (2010). Preservation of garnet growth zoning and the duration of prograde metamorphism. *Journal of Petrology*, 51, 2327–2347.
- Carlson, W. D. (1989). The significance of intergranular diffusion to the mechanism and kinetics of porphyroblast crystallization. *Contributions to Mineralogy and Petrology*, 103, 1–24.
- Carlson, W. D. (2006). Rates of Fe, Mg, Mn and Ca diffusion in garnet. *American Mineralogist*, 91, 1–11.
- Carlson, W. D. (2012). Rates and mechanism of Y, REE, and Cr diffusion in garnet. *American Mineralogist*, 97, 1598–1618.
- Chang, R., Neubauer, F., Liu, Y., Genser, J., Jin, W., Yuan, S., Guan, Q., Huang, Q., & Li, W. (2020). Subduction of a rifted passive continental margin: The Pohorje case of Eastern Alps—constraints from geochronology and geochemistry. *Swiss Journal of Geosciences*, 113, 14.
- Daniel, C. G., & Spear, F. S. (1999). The clustered nucleation and growth processes of garnet in regional metamorphic rocks from North-west Connecticut, USA. *Journal of Metamorphic Geology*, 17, 503–520.
- de Capitani, C., & Petrakakis, K. (2010). The computation of equilibrium assemblage diagrams with Theriak/Domino software. *American Mineralogist*, 95, 1006–1016.
- Diener, J. F. A., Powell, R., White, R. W., & Holland, T. J. B. (2007). A new thermodynamic model for clino- and orthoamphiboles in the system Na₂O-CaO-FeO-MgO-Al₂O₃-SiO₂-H₂O-O. *Journal of Metamorphic Geology*, 25, 631–656.
- Dragovic, B., Angiboust, S., & Tappa, M. J. (2020). Petrochronological close-up on the thermal structure of a paleo-subduction zone (W. Alps). *Earth and Planetary Science Letters*, 547, 116446.
- Duchêne, S., Blichert-Toft, J., Luais, B., Téluk, P., Lardeaux, J. M., & Albarède, F. (1997). The Lu-Hf dating of garnets and the ages of the Alpine high-pressure metamorphism. *Nature*, 387, 586–589.
- Faryad, S. W., & Henjes-Kunst, F. (1997). Petrological and K-Ar and ⁴⁰Ar-³⁹Ar age constraints for the tectonothermal evolution of the high-pressure Meliata unit, Western Carpathians (Slovakia). *Tectonophysics*, 280, 141–156.
- Faryad, S. W., Melcher, F., Hoinkes, G., Puhl, J., Meisel, T., & Frank, W. (2002). Relics of eclogite-facies metamorphism in the Austroalpine basement, Hochgrössen (Speik Complex), Austria. *Mineralogy and Petrology*, 74, 49–73.
- Fassmer, K., Obermüller, G., Nagel, T. J., Kirst, F., Froitzheim, N., Sandmann, S., Miladinova, I., Fonseca, R. O. C., & Münker, C. (2016). High-pressure metamorphic age and significance of eclogite-facies continental fragments associated with oceanic lithosphere in the Western Alps (Etirol-Levaz Slice, Valtourneche, Italy). *Lithos*, 252–253, 145–159.
- Fischer, G. W. (1978). Rate laws in metamorphism. *Geochimica et Cosmochimica Acta*, 42, 1035–1050.
- Frank, W. (1987). Evolution of the Austroalpine elements in the Cretaceous. In H. W. Flügel & P. Faupl (Eds.), *Geodynamics of the Eastern Alps* (pp. 379–406). Deuticke.
- Froitzheim, N., Schmid, S. M., & Frey, M. (1996). Mesozoic paleogeography and the timing of eclogite metamorphism in the Alps: A working hypothesis. *Eclogae Geologicae Helvetiae*, 89, 81–110.
- Ganguly, J., Cheng, W., & Chakraborty, S. (1998). Cation diffusion in aluminosilicate garnets: experimental determination in pyrope-almandine diffusion couples. *Contributions to Mineralogy and Petrology*, 131, 171–180.
- Godard, G., Martin, S., Prosser, G., Kienast, J. R., & Morten, L. (1996). Variscan migmatites, eclogites and garnet peridotites of the Ulten zone, Eastern Austroalpine system. *Tectonophysics*, 259, 313–341.
- Green, E. C. R., Holland, T. J. B., & Powell, R. (2007). An order-disorder model for omphacite pyroxenes in the system jadeite-diopside-hedenbergite-acmite with applications to eclogite rocks. *American Mineralogist*, 92, 1181–1189.
- Habler, G., Thöni, M., & Sölva, H. (2006). Tracing the high pressure stage in the polymetamorphic Texel Complex (Austroalpine basement unit, Eastern Alps): P-T-t-d constraints. *Mineralogy and Petrology*, 88, 269–296.
- Hamburger, M. W., Sarewitz, D. R., Pavlis, T. L., & Popandopulo, G. A. (1992). Structural and seismic evidence for intracontinental subduction in the Peter the First Range, Central Asia. *Geological Society of America Bulletin*, 104, 397–408.
- Hauke, M., Froitzheim, N., Nagel, T. J., Miladinova, I., Fassmer, K., Fonseca, R. O. C., Sprung, P., & Münker, C. (2019). Two high-pressure metamorphic events, Variscan and Alpine, dated by Lu-Hf in an eclogite complex of the Austroalpine nappes (Schobergruppe, Austria). *International Journal of Earth Sciences*, 108, 1317–1331.
- Hawthorne, F. C., Oberti, R., Harlow, G. E., Maresch, W. V., Martin, R. F., Schumacher, J. C., & Welch, M. D. (2012). IMA report, nomenclature of the amphibole supergroup. *American Mineralogist*, 97, 2031–2048.
- Hickmott, D. D., Shimizu, N., Spear, F. S., & Selverstone, J. (1987). Trace-element zoning in a metamorphic garnet. *Geology*, 15, 573–576.
- Hoinkes, G., Kostner, A., & Thöni, M. (1991). Petrologic constraints for Eo-Alpine eclogite facies metamorphism in the Austroalpine Ötztal basement. *Mineralogy and Petrology*, 43, 237–254.
- Hoke, L. (1990). The Altkristallin of the Kreuzeck Mountains, SE Tauern Window, Eastern Alps - basement crust in a convergent plate boundary. *Jahrbuch der Geologischen Bundesanstalt Wien*, 133, 5–87.
- Holland, T. J. B., & Powell, R. (1998). An internally consistent thermodynamic data set for phases of petrological interest. *Journal of Metamorphic Geology*, 16, 309–343.
- Hyppolito, T., Cambeses, A., Angiboust, S., Raimondo, T., Garcia-Casco, A., & Juliani, C. (2018). Rehydration of eclogites and garnet-replacement processes during exhumation in the amphibolite facies. *Geological Society, London, Special Publications*, 478, 217–239.
- Janák, M., Cornell, D., Froitzheim, N., De Hoog, J. C. M., Broska, I., Vrabec, M., & Hurai, V. (2009). Eclogite-hosting metapelites from the Pohorje Mountains (Eastern Alps): P-T evolution, zircon geochronology and tectonic implications. *European Journal of Mineralogy*, 21, 1191–1212.

- Janák, M., Froitzheim, N., Lupták, B., Vrabec, M., & Krogh Ravná, E. J. (2004). First evidence for ultrahigh-pressure metamorphism of eclogites in Pohorje, Slovenia: tracing deep continental subduction in the Eastern Alps. *Tectonics*, 23, TC5014.
- Janák, M., Froitzheim, N., Vrabec, M., Krogh Ravná, E. J., & De Hoog, J. C. M. (2006). Ultrahigh-pressure metamorphism and exhumation of garnet peridotite in Pohorje, Eastern Alps. *Journal of Metamorphic Geology*, 24, 19–31.
- Janák, M., Froitzheim, N., Yoshida, K., Sasinková, V., Nosko, M., Kobayashi, T., Hirajima, T., & Vrabec, M. (2015). Diamond in metasedimentary crustal rocks from Pohorje, Eastern Alps: A window to deep continental subduction. *Journal of Metamorphic Geology*, 33, 495–512.
- Jochum, K. P., Weiss, U., Stoll, B., Kuzmin, D., Yang, Q., Raczek, I., Jacob, D. E., Stracke, A., Birbaum, K., Frick, D. A., Günther, D., & Enzweiler, J. (2011). Determination of reference values for NIST SRM 610-617 glasses following ISO guidelines. *Geostandards and Geoanalytical Research*, 35, 397–429.
- Kellett, D. A., Cottle, J. M., & Smit, M. (2014). Eocene deep crust at Ama Drime, Tibet: Early evolution of the Himalayan orogen. *Lithosphere*, 6(4), 220–229.
- Konrad-Schmolke, M., Zack, T., O'Brien, P. J., & Jacob, D. E. (2008). Combined thermodynamic and rare earth element modelling of garnet growth during subduction: Examples from ultrahigh-pressure eclogite of the Western Gneiss Region, Norway. *Earth and Planetary Science Letters*, 272, 488–498.
- Konzett, J., Krenn, K., Hauzenberger, C., Whitehouse, M., & Hoinkes, G. (2012). High-pressure tourmaline formation and fluid activity in Fe-Ti-rich eclogites from the Kreuzeck Mountains, Eastern Alps, Austria. *Journal of Petrology*, 53, 99–125.
- Kretz, R. (1974). Some models for the rate of crystallization of garnet in metamorphic rocks. *Lithos*, 7, 123–131.
- Kromel, J., Putis, M., & Bacik, P. (2011). The Middle Austro-Alpine Siegraben structural complex—New data on geothermobarometry. *Acta Geologica Slovaca*, 3, 1–12.
- Kurz, W., & Fritz, H. (2003). Tectonometamorphic evolution of the Austroalpine Nappe Complex in the Central Eastern Alps—Consequences for the Eo-Alpine evolution of the Eastern Alps. *International Geology Review*, 45, 1100–1127.
- Ladenhauf, C., Armstrong, R. A., Konzett, J., & Miller, C. (2001). The timing of the pre-alpine HP-metamorphism in the Eastern Alps: constraints from U-Pb SHRIMP dating of eclogite zircons from the Austro-Alpine Silvretta nappe. *Geologische und Paläontologische Mitteilungen Innsbruck*, 25, 131.
- Lagos, M., Scherer, E. E., Tomaschek, F., Munker, C., Keiter, M., Berndt, J., & Ballhaus, C. (2007). High precision Lu-Hf geochronology of Eocene eclogite-facies rocks from Syros, Cyclades, Greece. *Chemical Geology*, 243, 16–35.
- Lichem, Ch., Hoinkes, G., & Gregurek, D. (1997). Polymetamorphism of the Austroalpine Koralm basement: new evidence for a Permian event. *Terra Nova Abstract 9 (Supplement 1)*, 489.
- Linner, M. (1999). Die P-T-t Entwicklung der Eklogite im Schoberkristallin als Beleg für frühalpide kontinentale Subduktion im Ostalpinen Kristallin. PhD Thesis, Institute of Petrology, University of Vienna, 167 pp.
- Longerich, H. P., Jackson, S. E., & Günther, D. (1996). Laser ablation inductively coupled plasma mass spectrometric transient signal data acquisition and analyte concentration calculation. *Journal of Analytical Atomic Spectrometry*, 11, 899–904.
- Ludwig, K. R. (2001). Isoplot/Ex version 2.49, Geochronological toolkit for Microsoft excel. Berkeley Geochronology Center Special Publications 1a.
- Miladinova, I., Froitzheim, N., Nagel, T. J., Janák, M., Georgiev, N., Fonseca, R. O. C., Sandmann, S., & Munker, C. (2018). Late Cretaceous eclogite in the Eastern Rhodopes (Bulgaria): Evidence for subduction under the Sredna Gora magmatic arc. *International Journal of Earth Sciences*, 107, 2083–2099.
- Miller, C. (1990). Petrology of the type locality eclogites from the Koralpe and Saualpe (Eastern Alps), Austria. *Schweizerische Mineralogische und Petrologische Mitteilungen*, 70, 287–300.
- Miller, C., Mundil, R., Thöni, M., & Konzett, J. (2005). Refining the timing of eclogite metamorphism: a geochemical, petrological, Sm-Nd and U-Pb case study from the Pohorje Mountains, Slovenia (Eastern Alps). *Contributions to Mineralogy and Petrology*, 150, 70–84.
- Miller, C., Stosch, H. G., & Hoernes, S. (1988). Geochemistry and origin of eclogites from the type locality Koralpe and Saualpe, Eastern Alps, Austria. *Chemical Geology*, 67, 103–118.
- Miller, C., & Thöni, M. (1995). Origin of eclogites from the Austroalpine Ötztal basement (Tirol, Austria): Geochemistry and Sm-Nd vs. Rb-Sr isotope systematics. *Chemical Geology*, 122, 199–225.
- Miller, C., & Thöni, M. (1997). Eo-Alpine eclogitisation of Permian MORB-type gabbros in the Koralpe (Eastern Alps, Austria): New geochronological, geochemical and petrological data. *Chemical Geology*, 137, 283–310.
- Miller, C., Thöni, M., Konzett, J., Kurz, W., & Schuster, R. (2005). Eclogites from the Koralpe and Saualpe type-localities, Eastern Alps, Austria. *Mitteilungen der Österreichischen Mineralogischen Gesellschaft*, 150, 227–263.
- Miller, C., Zanetti, A., Thöni, M., & Konzett, J. (2007). Eclogitisation of gabbroic rocks: redistribution of trace elements and Zr in rutile thermometry in an Eo-Alpine subduction zone (Eastern Alps). *Chemical Geology*, 239, 96–123.
- Munker, C., Weyer, S., Scherer, E. E., & Mezger, K. (2001). Separation of high field strength elements (Nb, Ta, Zr, Hf) and Lu from rock samples for MC-ICPMS measurements. *Geochemistry, Geophysics, Geosystems*, 2, 1064.
- Neubauer, F., Dallmeyer, R., & Takasu, A. (1999). Conditions of eclogite formation and age of retrogression within the Siegraben unit, Eastern Alps: Implications for Alpine-Carpathian tectonics. *Schweizerische Mineralogische und Petrologische Mitteilungen*, 79, 297–307.
- Neubauer, F., Genser, J., & Handler, R. (2000). The Eastern Alps: Result of a two-stage collision process. *Mitteilungen der Österreichischen Geologischen Gesellschaft*, 92, 117–134.
- Neubauer, F., & Höck, V. (2000). Aspects of geology in Austria and adjoining areas: introduction. *Mitteilungen der Österreichischen Geologischen Gesellschaft*, 92, 7–14.
- Neubauer, F., Hoinkes, G., Sassi, F. P., Handler, R., Höck, V., Koller, F., & Frank, W. (1999). Pre-Alpine metamorphism of the Eastern Alps. *Schweizerische Mineralogische und Petrologische Mitteilungen*, 79, 41–62.
- Page, F. Z., Essene, E. J., & Mukasa, S. B. (2003). Prograde and retrograde history of eclogites from the Eastern Blue Ridge,

- North Carolina, USA. *Journal of Metamorphic Geology*, 21, 685–698.
- Penniston-Dorland, S. C., Kohn, M. J., & Manning, C. E. (2015). The global range of subduction zone thermal structures from exhumed blueschists and eclogites: Rocks are hotter than models. *Earth and Planetary Science Letters*, 428, 243–254.
- Polino, R., Dal Piaz, G., & Gosso, G. (1990). Tectonic erosion at the Adria margin and accretionary processes for the Cretaceous orogeny of the Alps. *Mémoires de la Société Géologique de France*, 156, 345–367.
- Poupinet, G., Avouac, J., Jiang, M., Wei, S., Kissling, E., Herquel, G., Guilbert, J., Paul, A., Wittlinger, G., Su, H., Thomas, J.-C., & Thomas, J. (2002). Intracontinental subduction and Palaeozoic inheritance of the lithosphere suggested by a teleseismic experiment across the Chinese Tien Shan. *Terra Nova*, 14, 18–24.
- Roda, M., Spalla, M. I., & Marotta, A. M. (2012). Integration of natural data within a numerical model of ablative subduction: A possible interpretation for the Alpine dynamics of the Austroalpine crust. *Journal of Metamorphic Geology*, 30, 973–996.
- Sandmann, S., Herwartz, D., Kirst, F., Froitzheim, N., Nagel, T. J., Fonseca, R. O. C., Münker, C., & Janák, M. (2016). Timing of eclogite-facies metamorphism of mafic and ultramafic rocks from the Pohorje Mountains (Eastern Alps, Slovenia) based on Lu-Hf garnet geochronometry. *Lithos*, 262, 576–585.
- Scherer, E. E., Cameron, K. L., & Blichert-Toft, J. (2000). Lu-Hf garnet geochronology: Closure temperature relative to the Sm-Nd system and the effects of trace mineral inclusions. *Geochimica et Cosmochimica Acta*, 64, 3413–3432.
- Scherer, E. E., Münker, C., & Mezger, K. (2001). Calibration of the Lutetium-Hafnium clock. *Science*, 293, 683–687.
- Schmid, S. M., Fügenschuh, B., Kissling, E., & Schuster, R. (2004). Tectonic map and overall architecture of the Alpine orogen. *Eclogae Geologicae Helveticae*, 97, 93–117.
- Schulz, B. (1993). Mineral chemistry, geothermobarometry and pre-Alpine high-pressure metamorphism of eclogitic amphibolites and mica schists from the Schobergruppe, Austroalpine Basement, Eastern Alps. *Mineralogical Magazine*, 57, 189–202.
- Schuster, R., Scharbert, S., Abart, R., & Frank, W. (2001). Permo-Triassic extension and related HT/LP metamorphism in the Austroalpine—Southalpine realm. *Mitteilungen der Gesellschaft der Geologie- und Bergbaustudenten in Österreich.*, 45, 111–141.
- Schuster, R., & Stüwe, K. (2008). Permian metamorphic event in the Alps. *Geology*, 36, 603–606.
- Skora, S., Baumgartner, L. P., Mahlen, N. J., Johnson, C. M., Pilet, S., & Hellebrand, E. (2006). Diffusion-limited REE uptake by eclogite garnets and its consequences for Lu-Hf and Sm-Nd geochronology. *Contributions to Mineralogy and Petrology*, 152, 703–720.
- Skora, S., Mahlen, N., Baumgartner, L. P., Johnson, C., & Pilet, S. (2005). Garnet zoning pattern, growth mechanisms and the development of Lu-depleted halos in eclogites. *Geochimica et Cosmochimica Acta*, 10(Suppl 69), 403.
- Smit, M., Scherer, E., & Mezger, K. (2013). Lu-Hf and Sm-Nd garnet geochronology: chronometric closure and implications for dating petrological processes. *Earth and Planetary Science Letters*, 381, 222–233.
- Smit, M. A., Scherer, E. E., John, T., & Janssen, A. (2011). Creep of garnet in eclogite: Mechanisms and implications. *Earth and Planetary Science Letters*, 311, 411–419.
- Sobel, E. R., Chen, J., Schoenbohm, L. M., Thiede, R., Stockli, D. F., Sudo, M., & Strecker, M. R. (2013). Oceanic-style subduction controls late Cenozoic deformation of the Northern Pamir orogen. *Earth and Planetary Science Letters*, 363, 204–218.
- Söderlund, U., Patchett, P. J., Vervoort, J. D., & Isachsen, C. E. (2004). The ¹⁷⁶Lu decay constant determined by Lu-Hf and U-Pb isotope systematics of Precambrian mafic intrusions. *Earth and Planetary Science Letters*, 219, 311–324.
- Sölva, H., Thöni, M., Grasemann, B., & Linner, M. (2001). Emplacement of eo-Alpine high-pressure rocks in the Austroalpine Ötztal Complex (Texel Group, Italy/Austria). *Geodinamica Acta*, 14, 345–360.
- Spear, F. S., & Daniel, C. G. (1998). 3-dimensional imaging of garnet porphyroblast sizes and chemical zoning: Nucleation and growth history in the garnet zone. *Geological Materials Research*, 1, 1–44.
- Spear, F. S., & Daniel, C. G. (2001). Diffusion control of garnet growth, Harpswell Neck, Maine USA. *Journal of Metamorphic Geology*, 19, 179–195.
- Stern, R. J. (2004). Subduction initiation: Spontaneous and induced. *Earth and Planetary Science Letters*, 226, 275–292.
- Stüwe, K., & Schuster, R. (2010). Initiation of subduction in the Alps: Continent or ocean? *Geology*, 38, 175–178.
- Tenczer, V., & Stüwe, K. (2003). The metamorphic field gradient in the eclogite type locality Koralpe region, Eastern Alps. *Journal of Metamorphic Geology*, 21, 377–393.
- Thöni, M. (1983). The thermal climax of the early Alpine metamorphism in the Austroalpine thrust sheet. *Sciences Géologiques – Mémoires*, 36, 211–238.
- Thöni, M. (1999). A review of geochronological data from the Eastern Alps. *Schweizerische Mineralogische und Petrologische Mitteilungen*, 79, 209–230.
- Thöni, M., & Jagoutz, E. (1992). Some new aspects of dating eclogites in orogenic belts: Sm-Nd, Rb-Sr, and Pb-Pb isotopic results from the Austroalpine Saualpe and Koralpe type locality (Carinthia/Styria, southeastern Austria). *Geochimica et Cosmochimica Acta*, 56, 347–368.
- Thöni, M., & Jagoutz, E. (1993). Isotopic constraints for eo-Alpine high-P metamorphism in the Austroalpine nappes of the Eastern Alps: Bearing on Alpine orogenesis. *Schweizerische Mineralogische und Petrographische Mitteilungen*, 73, 177–189.
- Thöni, M., & Miller, C. (1996). Garnet Sm-Nd data from the Saualpe and the Koralpe (Eastern Alps, Austria): Chronological and PT constraints on the thermal and tectonic history. *Journal of Metamorphic Geology*, 14, 453–466.
- Thöni, M., Miller, C., Blichert-Toft, J., Whitehouse, M. J., Konzett, J., & Zanetti, A. (2008). Timing of high-pressure metamorphism and exhumation of the eclogite type-locality (Kupplerbrunn-Prickler Halt, Saualpe, south-eastern Austria): constraints from correlations of the Sm-Nd, Lu-Hf, U-Pb and Rb-Sr isotopic systems. *Journal of Metamorphic Geology*, 26, 561–581.
- Tirone, M., Ganguly, J., Dohmen, R., Langenhorst, F., Hervig, R., & Becker, H.-W. (2005). Rare earth diffusion kinetics in garnet: Experimental studies and applications. *Geochimica et Cosmochimica Acta*, 69, 2385–2398.

- Tropper, P., Essene, E. J., Sharp, Z. D., & Hunziker, J. C. (1999). Application of K-feldspar-jadeite-quartz barometry to eclogite facies metagranites and metapelites in the Sesia Lanzo Zone (Western Alps, Italy). *Journal of Metamorphic Geology*, *17*, 195–209.
- Tumiati, S., Thöni, M., Nimis, P., Martin, S., & Mair, V. (2003). Mantle–crust interactions during Variscan subduction in the Eastern Alps (Nonsberg–Ulten Zone); geochronology and new petrological constraints. *Earth and Planetary Science Letters*, *210*, 509–526.
- van Orman, J., Grove, T., Shimizu, N., & Layne, G. (2002). Rare earth element diffusion in a natural pyrope single crystal at 2.8 GPa. *Contributions to Mineralogy and Petrology*, *142*, 416–424.
- Vrabec, M., Janák, M., Froitzheim, N., & De Hoog, J. C. M. (2012). Phase relations during peak metamorphism and decompression of the UHP kyanite eclogites, Pohorje Mountains (Eastern Alps, Slovenia). *Lithos*, *144*, 40–55.
- Warren, C. J. (2013). Exhumation of (ultra-)high-pressure terranes: Concepts and mechanisms. *Solid Earth*, *4*, 75–92.
- White, R. W., Powell, R., & Holland, T. J. B. (2007). Progress relating to calculation of partial melting equilibria for metapelites. *Journal of Metamorphic Geology*, *25*, 511–527.
- Wiesinger, M., Neubauer, F., & Handler, R. (2006). Exhumation of the Saualpe eclogite unit, Eastern Alps: constraints from $^{40}\text{Ar}/^{39}\text{Ar}$ ages and structural investigations. *Mineralogy and Petrology*, *88*, 149–180.
- Yamato, P., Agard, P., Burov, E., Le Pourhiet, L., Jolivet, L., & Tiberi, C. (2007). Burial and exhumation in a subduction wedge: Mutual constraints from thermomechanical modeling and natural P-T-t data (Schistes Lustrés, western Alps). *Journal of Geophysical Research*, *112*, B07410.
- Zack, T., & Kooijman, E. (2017). Petrology and geochronology of rutile. *Reviews in Mineralogy and Geochemistry*, *83*, 443–467.
- Zanchetta, S. (2007). Evoluzione tettonometamorfica delle unita' di Texel e dello Schneeberg (Alpi centro-orientali). *Rendiconti Online della Società Geologica Italiana*, *4*, 312–314.
- Zanchetta, S., Poli, S., Rubatto, D., Zanchi, A., & Bove, G. M. (2013). Evidence for deep subduction of Austroalpine crust (Texel Complex, NE Italy). *Rendiconti Lincei: Scienze Fisiche e Naturali*, *24*, 163–176.

SUPPORTING INFORMATION

Additional supporting information may be found in the online version of the article at the publisher's website.

Data S1. Supporting information

Figure S1. Equilibrium phase diagram calculated for SiAlFeMgCaNaOH bulk composition of the dated eclogite sample HO 1. Additionally, compositional isopleths for almandine (red lines) and grossular (green lines) components in garnet were calculated. Grey isopleths show volume percentage of garnet. The yellow star corresponds to the estimated peak conditions. For more details see “P-T estimates”.

Figure S2. Equilibrium phase diagram calculated for SiAlFeMgCaNaOH bulk composition of the dated eclogite sample HO 2. Additionally, compositional isopleths for grossular (green lines) and pyrope (blue lines) components in garnet were calculated. The yellow star corresponds to the estimated peak conditions. For more details see “P-T estimates”.

Figure S3. Equilibrium phase diagram calculated for SiAlFeMgCaNaOH bulk composition of the dated eclogite sample GRÜ 2. Additionally, compositional isopleths for almandine (red lines) and grossular (green lines) components in garnet were calculated. Grey isopleths show volume percentage of garnet. The yellow star corresponds to the estimated peak conditions. For more details see “P-T estimates”.

Figure S4. Equilibrium phase diagram calculated for SiAlFeMgCaNaOH bulk composition of the dated eclogite sample WOL 1. Additionally, compositional isopleths for almandine (red lines) and grossular (green lines) components in garnet were calculated. Grey isopleths show volume percentage of garnet. The yellow star corresponds to the estimated peak conditions. For more details see “P-T estimates”.

Figure S5. Equilibrium phase diagram calculated for SiAlFeMgCaNaOH bulk composition of the dated eclogite sample SIG 3. Additionally, compositional isopleths for almandine (red lines) and grossular (green lines) components in garnet were calculated. Grey isopleths show volume percentage of garnet. The yellow star corresponds to the estimated peak conditions. For more details see “P-T estimates”.

Figure S6. Equilibrium phase diagram calculated for SiAlFeMgCaNaOH bulk composition of the dated eclogite sample SAL 1. Additionally, compositional isopleths for almandine (red lines) and grossular (green lines) components in garnet were calculated. Grey isopleths show volume percentage of garnet. The yellow star corresponds to the estimated peak conditions. For more details see “P-T estimates”.

How to cite this article: Miladinova, I., Froitzheim, N., Nagel, T. J., Janák, M., Fonseca, R. O. C., Sprung, P., & Münker, C. (2022). Constraining the process of intracontinental subduction in the Austroalpine Nappes: Implications from petrology and Lu-Hf geochronology of eclogites. *Journal of Metamorphic Geology*, *40*(3), 423–456. <https://doi.org/10.1111/jmg.12634>